2014-12-31

Design And Development Of The Portable Build Platform And Heated Travel Envelope For The Multi3d Manufacturing System

Steven Daniel Ambriz
University of Texas at El Paso, sdambriz@miners.utep.edu

DESIGN AND DEVELOPMENT OF THE PORTABLE BUILD PLATFORM AND HEATED TRAVEL ENVELOPE FOR THE MULTI^{3D} MANUFACTURING SYSTEM

STEVEN DANIEL AMBRIZ

Department of Mechanical Engineering

APPROVED:

Ryan Wicker, Ph.D., Chair

Yirong Lin, Ph.D.

David Roberson, Ph.D.

Charles Ambler, Ph.D.
Dean of the Graduate School

Dedication

This thesis is dedicated to my wife, my parents, and my siblings for their continuous support throughout my academic career.

DESIGN AND DEVELOPMENT OF THE PORTABLE BUILD PLATFORM AND HEATED TRAVEL ENVELOPE FOR THE MULTI^{3D} MANUFACTURING SYSTEM

by

STEVEN DANIEL AMBRIZ, B.S. in Mechanical Engineering

THESIS

Presented to the Faculty of the Graduate School of

The University of Texas at El Paso

in Partial Fulfillment

of the Requirements

for the Degree of

MASTER OF SCIENCE

Department of Mechanical Engineering

THE UNIVERSITY OF TEXAS AT EL PASO

December 2015

Acknowledgements

I would like to express my gratitude to my advisor and committee chair in this work, Dr. Ryan Wicker, the director of the W.M. Keck Center for 3D innovation (Keck Center) for his continuous support, mentorship and constructive criticism throughout my research as a graduate student. Mr. David Espalin, associate director also deserves great recognition for his mentorship during my research. I am greatly indebted to him for his vast contribution to my development as a professional, contribution of ideas and technical assistance, and constant encouragement. The research work contained in this publication would not have been possible without the state-of-art facilities that have been established by Dr. Wicker and the other faculty and staff of the Keck Center. As well, I would like extend my appreciation to my committee members, Dr. Yirong Lin and Dr. David Roberson.

Additionally, I would like to acknowledge America Makes, the National Additive Manufacturing Innovation Institute, which funded this project. America Makes is funded by the Office of the Secretary of Defense, Manufacturing and Industrial Base Policy, Manufacturing Technology, through a cooperative agreement with the Air Force Research Laboratory (FA8650-12-2-7230). I would also like to acknowledge Northrop Grumman, rp+m, Lockheed Martin, the University of New Mexico and Youngstown State University for their contributions in this project. I would also like to thank Stratasys, specifically Mr. Bob Zinniel for his technical support during the mechanical modifications of the FDM machines and providing an understanding of the FDM process and Mr. Ron Schloesser for his technical support that enabled communication and control of the FDM machines.

Other various individuals of the Keck Center also deserve recognition. I would like to extend my gratitude to Mr. Jose L. Coronel for his major contribution in the development of this

system via implementation of the robotics and control systems. I would like to thank undergraduate students Mr. Alfonso Fernandez, Mr. Jorge Ramirez, Mr. Alex Cuaron, Mr. Juan Vargas, Mr. Jose Motta, and Mr. Christopher Minjares for their help with machining components and for other technical support they provided in this work. As well I would like to thank other faculty, staff, and students of the Keck Center for their support in this project. I would like to thank Mr. Fernando Arras of Centertech CNC Machining for his support in machining the base of the portable build platform. In addition, I would like to extend a special thanks to Dr. Benjamin Flores, Dr. Helmut Knaust, Mrs. Ariana Arcerio-Pino, and Mrs. Sara Rodriguez of the University of Texas System Louis Stokes Alliance for Minority Participation (LSAMP) program for support via the National Science Foundation Bridge to the Doctorate Fellowship (NSF grant number HRD-1301858).

Finally, last but not least, I would like to thank my wife, Iris for her understanding, continuous support and love which ultimately made this thesis work possible. I would also like to thank my parents, Lourdes and Frank, siblings, Frankie, Ashley and Victoria, and other family and friends for constantly supporting and encouraging me during the pursuit of my graduate degree.

Abstract

The final product functionality of parts produced by Additive Manufacturing (AM) can, in part, be improved by the inclusion of multi-material capabilities. The "Multi^{3D} system" that is under development at The University of Texas at El Paso uses material extrusion printing (or fused deposition modeling), solid conductor wire embedding, direct-write, component placement, and micromaching to enable multi-material fabrication. The Multi^{3D} was designed to transport a workpiece between manufacturing stations via a six-axis robot, portable build platform (PBP), and a controlled temperature environment or chamber that travels to each manufacturing station. The heated travel envelope (HTE) was included to mitigate thermal shrinkage (and eventually warping) that occurs when a thermoplastic is subjected to a decrease in temperature within a short time frame. An end-effector was also designed to allow the six-axis robot to interact and handle the PBP and HTE.

Discussed in this work is the design and construction of the HTE as well as its performance in terms of maintaining a stable temperature while considering the imposed weight and dimensional constraints. The HTE design includes a compressible high temperature bellow "door" which allows it slide over builds and increases the height of builds (~22 cm) which can be produced in the Multi^{3D} system. The HTE is capable of maintaining a 150 ± 8°C environment with its convective heating system, which is the baseline set for building parts with polycarbonate, specifically 145°C. The temperature change (drop) of parts is reduced by 71% with the inclusion of HTE in the transportation process. The quantified temperature drop without the HTE during transportation was approximately 21 °C in comparison to 6 °C with the HTE.

The construction and performance (e.g., locating accuracy) of the PBP are also discussed. The PBP was designed around the "Platen" build platform to replicate its abilities but in a form

that allows it to be portable. The PBP is able to receive vacuum (-42.3 ±8.5 KPa) supply for restraining sacrificial build sheets in two forms, from the station of the Multi^{3D} system it is placed in and from the end-effector. The PBP locates accurately into the FDM system, in a form that maintains the FDM's achievable accuracy of ±38 μm, via the use of three locating pins and its vacuum fitting. The locating accuracy of the PBP was determined by printing "stair step" parts which were analyzed for layer shifting. These results were compared to stair steps printed in an unmodified FDM system as a control. The layer shifting was measured to be +50.8 to -38.1μm for non-paused builds and +63.5 to -50.8 μm for paused builds on both machines (modified and control). This gave indication that the modifications done to the FDM machine and the portable build platform had no direct effect on the achievable accuracy in parts with this specific geometry and these processing conditions.

Ultimately, the Multi^{3D} system will be utilized for Aerospace applications to manufacture components for Unmanned Aerial Vehicles (UAVs) and satellites, but other applications where disparate materials are required can be envisioned. This can be accomplished with these components or subsystems which were developed for material handling within the system.

Table of Contents

List of Tables

List of Figures

Chapter 1
Introduction

1.1 Background

Additive Manufacturing (AM), otherwise known as rapid prototyping and 3D printing, is a production process that implements a layer-by-layer approach to fabricate complex 3D objects from computer design files. Advances in the field of AM have given designers the ability to rapidly generate initial prototypes from concept designs. In the past 20 years, research in AM has produced novel processes which have been implemented in various fields such as automotive, biomedical, aerospace, and more. Recently, the fabrication of functional "end-use" products has been a popular trend in the AM field (Guo and Leu 2013). End-use products could entail parts that are multi-functional after printing, with more than a structural or aesthetic application. One particular application of interest is electro-mechanical functionality.

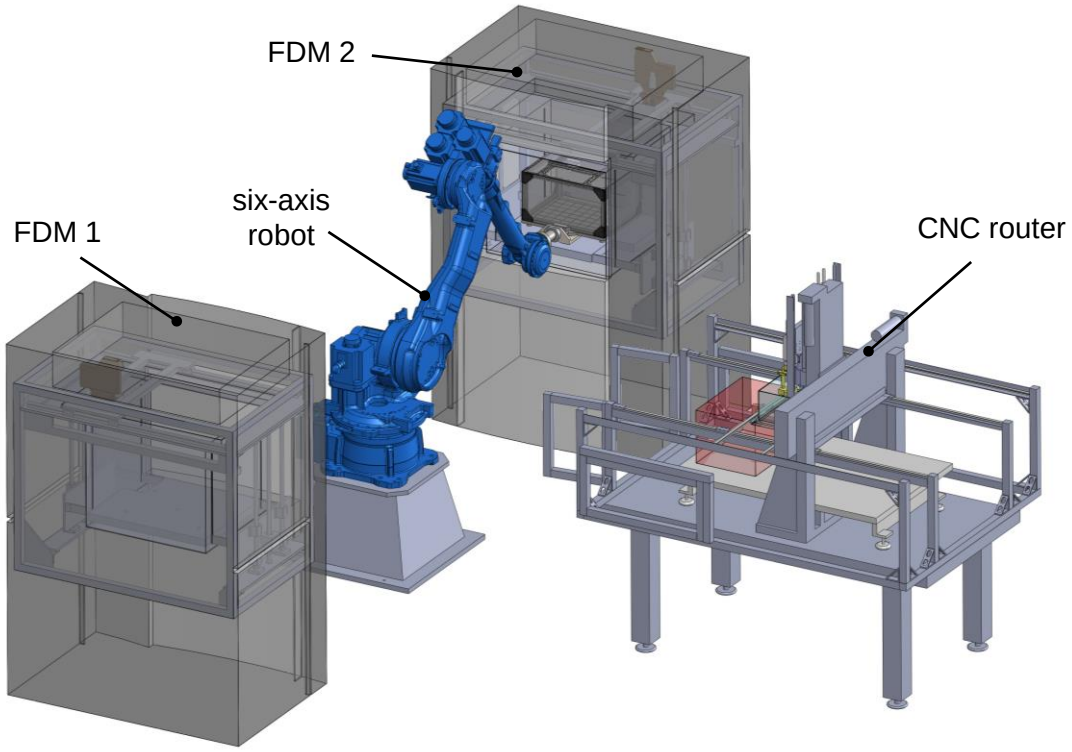

Figure 1.1. Multi^{3D} system CAD concept

The project involves research in the construction of a hybrid technology, the Multi^{3D} Manufacturing system, which will incorporate material extrusion printers, subtractive manufacturing, and other various capabilities. The system will enable the construction of multi-functional products with embedded electronics. The overall project goal is to develop a manufacturing process specifically containing FDM technology, CNC routing, direct-write, wire embedding, machine vision, and a six-axis robot. These capabilities will enable the design and manufacture of novel aerospace components such as UAVs and small satellites. Multiple FDM technologies will enable multi-material capabilities in the Multi3D system, which can lead to other various applications where disparate materials are required.

1.2 Motivation

The W.M. Keck Center for 3D Innovation (Keck Center) has conducted innovative practices in the past which involve the production of additively manufactured parts with embedded electronics. The goals of this research project in general have further matured these type of practices by directly minimizing human interaction in the development of such products. The Keck Center has conducted research in creating a system similar to the Multi^{3D} system with legacy FDM systems but issues with registration were encountered (Espalin, et al. 2014). These issues were attributed to the significant amount of modifications that were made to the legacy FDM systems. The concept of the Multi^{3D} system looked to overcome the limitations of the previous version. As a result, the use of a six axis robot to handle and transport the products was hypothesized to resolve these registration issues. The robot and portable build platform have reduced the amount of modifications needed to create the multi-functional system.

In order to reduce the amount of modifications required, it was important to not disturb the current process and checks or sensing the Fortus 400mc employs during printing. There are several

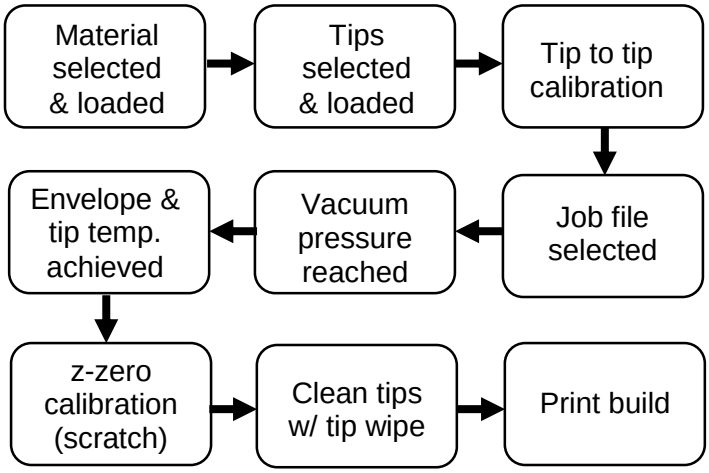

Figure 1.2. Fortus 400mc printing process

procedures or checks that the Fortus 400mc printer runs through prior to initializing a print. This includes calibration sequences for the tips and z stage "zero", temperature sensing and vacuum sensing. Figure 1.2 shows a basic outline of the steps followed in the process.

One of the most significant aspects of this project was the methodology used for material handling. The success of the project relied heavily on the ability to transport workpieces between the stations of the manufacturing system in repeatability manner. The six axis robot was a central factor of importance in this material handling process, but it could not complete the goal on its own. Three particular components are required to transport and appropriately handle the parts created by the system. A platform that was portable and capable of constraining the parts was required, the portable build platform (PBP). An oven or heated travel envelope (HTE) was required to transport parts in a heated environment, which is necessary for parts printed with FDM technology (Sun, et al. 2008). The heated environment mitigated thermal shrinkage that leads to warping in parts over time. Finally, an end-effector or "hand" for the robot arm was necessary to allow the robotic system to interact and "grip" the portable platform and envelope individual or together in an assembly.

1.3 Thesis Outline

The following material of this thesis document was organized into five chapters. Chapter 2 consists of an overview of Additive Manufacturing and FDM technology, along with literature review on topics correlated to the development process behind the material handling components. The review includes overview on the FDM build envelope patent, temperature history of FDM parts, and fixture design. Chapter 3 describes in detail the design and development process of the PBP, HTE, and end-effector. In Chapter 4 experimentation used to evaluate the prototype designs is reviewed. The results of these experiments are analyzed and the necessary design changes determined based on these results are detailed. Finally, conclusions and potential future work concerning this project are discussed in Chapter 5.

Chapter 2

Literature Review

2.1 Additive Manufacturing

Additive Manufacturing (AM) is a fabrication process that produces complex three-dimensional objects in a layer-by-layer approach (ASTM Standard F2792 −12a 2012). The part fabrication process with AM technology typically involves eight steps; 1) development of a 3D CAD model, 2) conversion of CAD model to STL format, 3) transfer of STL to AM machine and generation of tooling paths, 4) AM machine setup (material loading, calibration, etc.), 5) part building via layer by layer approach, 6) removal of part from the AM machine, 7) post processing of part, and 8) application of part. Several AM technologies exist and are developed by various companies. These technologies employ different strategies in part manufacturing, but still utilize the same layer-by-layer approach. The most commonly known technologies are shown in Table 2.1, along with the typical material types used in each technology (Guo and Leu 2013).

Table 2.1. AM technologies and typical material types used by each

AM Process	Typical material types
Binder jetting	Metals, polymers, plastics
Directed energy deposition	Polymers, ceramics, metals
Material extrusion	Thermoplastics, waxes
Material Jetting	Polymers, plastics
Powder bed fusion	Metals, polymers
Sheet lamination	Paper, plastics, metals
Vat photopolymerization	UV curable resin, acrylic plastic, waxes

Initially, the applications of additive manufacturing technologies were limited to merely prototyping purposes, as the outdated terminology of "rapid prototyping" suggests. Several applications have arisen since the introduction of the AM technologies, which extend beyond prototyping. The automotive manufacturing industry has used AM technology to produce new products for the market in a timely manner by using the technology to make parts available prior to the establishment of full production tools. The medical industry has used AM technology to produce physical solid objects from 3D medical imaging data which allows for individual customization for each patient (Campbell, Bourell and Gibson 2012).

2.2 Fused Deposition Modeling

Fused Deposition Modeling (FDM) is an AM material extrusion technology developed by Stratasys, Inc. used to build functional prototypes (Novakova-Marcincinova 2012). The technology has continued to develop and advance over the years, but it still stays consistent in its process and main components. The FDM technology process involves the production of three-dimensional objects, generated from Computer Aided Design (CAD) packages, by dispensing individual layers of molten thermoplastic filament through a temperature controlled nozzle. These layers are deposited into a prescribed pattern (x and y axes) onto a build platform. After the semi-molten filament is deposited in a layer, the build platform moves down (z-axis) an increment equivalent to the height of the previous layer and deposits the preceding layer. The semi-molten filament solidifies and cools as it continues to deposit and bonds with the adjoining layer of material. A FDM printer typically contains two extruder head nozzles, one for the modeling filament and another for the support material (Sun, et al. 2008), which is required for supporting complex and overhanging features.

FDM technology enables many advantages over traditional production processes (e.g., injection molding, blow molding, extrusion). Complex geometries can be easily constructed by

FDM technology, unlike in traditional processes where feature complexity is limited and adds cost due to expensive tooling. Mass customization is possible with FDM which can enable parts to more accurately serve their engineering purpose. An example of customization with FDM can be seen in a study conducted by Tuck, et al. in 2008 where customization facilitated by AM was utilized to customize seating profiles in aircraft ejection seats to improve individual comfort. Since FDM uses CAD modeling to create the structure of the parts, quick design changes are possible and lead times are shortened. Shortened lead times and other factors such as less production labor and less material waste, reduce production expenses (Shulman, Spradling and Hoag 2012). AM technologies in general can be more cost effective when parts are produced in low volume (Mellor, Hao and Zhang 2014).

Although the FDM process provides significant advantages over other processes, the parts produced by this process contain limitations and challenges are faced in promoting the industry wide adoption of the technology. Although AM technologies are more cost effective in lower level production, they become less cost effective when mass producing products due to operation time, material cost, and machine cost (Mellor, Hao and Zhang 2014). Surface roughness is among the disadvantages produced in the products of technology. The roughness is caused by the unavoidable stair-stepping effect which is related to the layer-by-layer manufacturing principle (Armillotta 2006). Another significant limitation that is apparent is the interlayer bonding within the products, leading to porous parts. The quality of the bonds is an influential factor in determining the produced part's overall structural integrity. Studies have shown that insufficient bond strength between the filaments negatively influence the mechanical properties of the parts (Sun, et al. 2008). One of the most prominent focuses of research in FDM technology and the AM field in general,

is the production of multi-material (Sugavaneswaran and Arumaikkannu 2014) and multi-functional parts (Guo and Leu 2013).

2.3 High temperature modeling apparatus, FDM build envelope patent

Fused Deposition Modeling technologies developed by Stratasys center around what is called a "high temperature modeling apparatus." The modeling apparatus contains the components typical to the FDM printing process, such as the dispensing head, z-gantry, build platform, and heated build chamber. This heated build chamber of the modelling apparatus is also known as the build envelope. The heated build envelope encompasses printed parts in a high temperature environment to relieve the stresses caused by cooling of the filament after it is extruded (Swanson, et al. 2004).

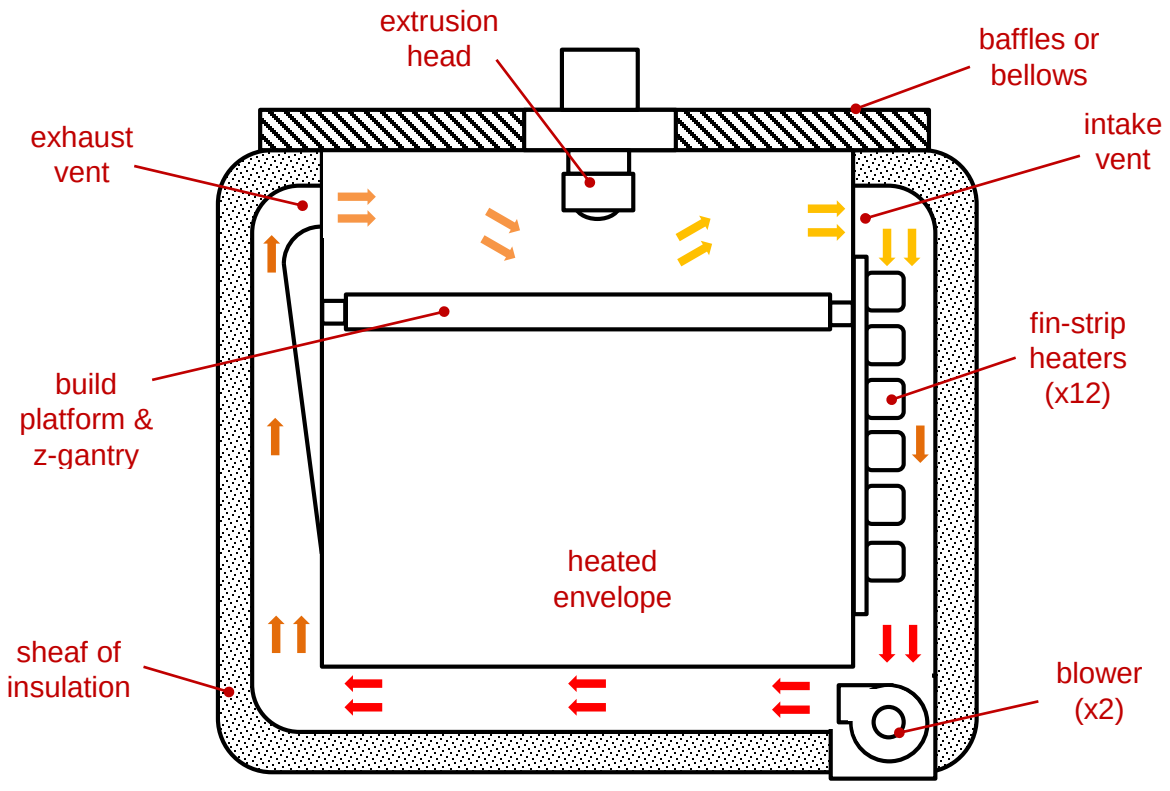

Figure 2.2 Diagram of Stratasys' high temperature modeling apparatus heating system, front sectioned view

The heating system for the build envelope uses forced convection to recirculate and heat the environment inside the envelope. The build envelope's bottom, left, and right walls are surrounded by a duct and two vents for the ducting are located at the top of the left wall and the top of the right wall. Within in the ducting of the right wall, two banks of six fin-strip heaters are mounted. Two air blowers are located in the ducting at the bottom right corner, so that the blowers intake the air from the right wall ducting and exhaust air through the bottom ducting to left wall ducting, as shown in Figure 2.2. As a result, the vent on the right side wall is used to intake air from the envelope and the vent of the left side wall is used to exhaust air to the envelope. This causes air flow to recirculate in a clockwise direction and air to be heated through convection as it passes through the heaters. A thermocouple is placed in front of the intake vent to monitor the temperature of the envelope.

Table 2.2. Maximum envelope and extrusion temperature for thermoplastics

Material	Maximum envelope temperature (°C)	Maximum extrusion temperature (°C)
ABS-M30/M30i	95	320
Nylon12	120	355
PC/PC-ISO	145	390
PC-ABS	110	330
PPSF	225	405
ULTEM 9085	190	400

The dispensing head of the FDM technology is able to move in an x-y plane via a servo motor controlled gantry. The ceiling of the build envelope, where the extrusion head is located, is comprised of two baffles, which are thermally insulated and deformable. One baffle is used for x plane movement and the other for y plane movement. The baffles allow movement of the extrusion head avoiding unfavorable heat loss from the build envelope. FDM technologies developed by Stratasys are capable of printing with several thermoplastics with different properties. The

envelope temperature and extrusion temperatures are altered for printing with each thermoplastic. The Fortus 400mc, the FDM technology employed in the Multi^{3D} system, can print with the thermoplastics seen in Table 2.2 and the processing temperatures are also shown.

The methodology employed in specific aspects of the high temperature modeling apparatus was used to guide certain design features of the HTE. Specifically, the recirculating convection heating methodology via finned strip heaters used by the high temperature modeling apparatus was used to guide the design of the HTE's heating system. As well, the use of high temperature baffles or bellows to thermally insulate the ceiling of build chamber was used to guide the design of the actuating door of the HTE. These design features are further discussed in a later section of document.

2.4 Temperature history of FDM parts

The temperature history or profile of extruded filament interfaces in FDM products is significant to the formation of bonds. Through experimentation, it is seen that the quality of bonds achieved between adjacent filament layers is affected by processing conditions such as envelope temperature and convective conditions. Consequently, the overall mechanical properties of the products are directly affected by bond strength (Sun, et al. 2008). This phenomena was important to consider when working towards the development of the Multi^{3D} system. Maintaining part quality was essential when developing such a technology that looks to diversify the applications of FDM built parts.

Sun, et al. in 2008 conducted a study that analyzed the effects of processing parameters on bond quality in FDM built parts. Among these parameters, convective conditions and envelope temperature were considered. Mesostructure characteristics and mechanical properties were used to characterize the bond quality in these parts. Mesostructure of the FDM parts was characterized

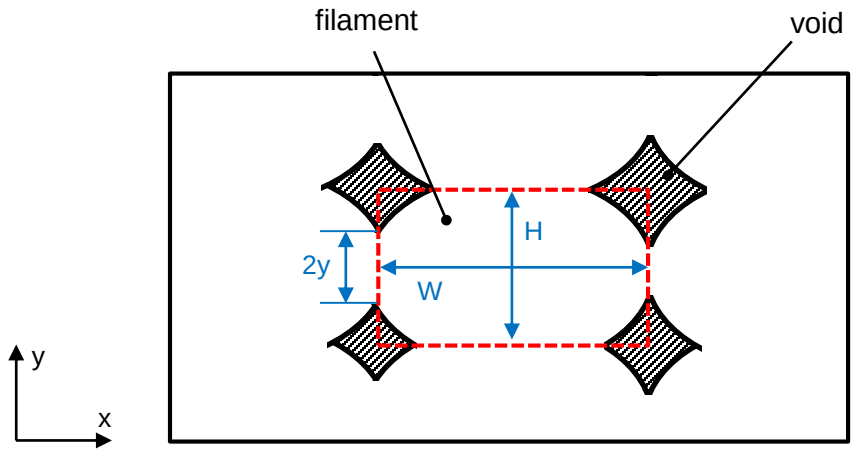

Figure 2.3 Illustration of FDM substrate cross-sectional view where W is width of a filament and H is height and neck growth between adjacent filaments is 2y

by neck growth (2y) between adjacent filaments, which is value that indicates the entanglement of them. Neck growth data was obtained via cross-sectioning of specimens, image capture of cross-sections under an optical microscope and features were analyzed via software. Figure 2.3 shows an illustration of a cross-sectioned specimen, which labels the dimensions of the filament (height and width) and the neck growth (2y). Mechanical properties were analyzed via three-point bending testing to produce flexural strength data. The material of investigation in this study was acrylonitrile butadiene styrene (ABS) P400 and a FDM 2000 printer was used. Three envelope temperatures were considered, 50, 60 and 70°C. Analysis of flexural strength showed a large standard deviation in data when considering samples produced with the same processing conditions (24 samples per set). It was observed that the build location played a large role in this deviation. As a result, temperature profiles were obtained from parts built at different locations on the platform. From the results recorded, the base temperature of parts in varying locations ranged from approximately 100 to 140°C (33% difference). Necking growth was observed to be 31 percent greater in part observed to have the highest base temperature (Part 9) when compared to the part with the lowest base temperature (Part 1). Flexural strength was reported via average

failure load, which ranged from 185.5 to 233.1 N. This indicates a 26 percent increase in flexural strength due to 31 percent greater neck growth caused by a higher temperature profile.

Improving the thermal distribution within the FDM envelope was not a goal during the development of the Multi^{3D} system. As well, the temperature profile experienced with the FDM 2000 cannot be fully comparable to a newer FDM technology, the Fortus 400mc. The main aspect that was taken away from this publication was the part cooling experienced in the varying build locations had strong effects on bond quality. Therefore, having taken into consideration the implications of part cooling on part quality/strength, the goal was to avoid major cooling and temperature fluctuation during part transport in the Multi^{3D} system. This was the central reasoning in including the HTE component during material handling/transport.

2.5 Fixture design, locating methodology

Fixtures are defined as components that are designed to locate and brace workpieces during manufacturing processes. The design of fixtures heavily influences the quality of manufacturing. Two categories exist that define fixture types, dedicated fixtures and modular fixtures. Each category can utilize ordinary fixture components such as supports, clamps, and locators. Dedicated fixtures are composed of these fixture components or custom ones and are designed for specific workpieces. Modular fixtures consist of various combinations and configurations of these components to accommodate for diverse workpieces. Dedicated fixtures are generally used for mass production because of their specially designed characteristics, while modular fixtures are used for low-volume production (Rong and Huang 2005).

The methodology of designing fixtures can be divided into three steps: 1) setup planning, 2) fixture planning, and 3) fixture configuration. Setup planning involves the determination of the required number of setups, workpiece orientation and position in each setup, and the machining

surfaces of each setup. During fixture planning, the locating, clamping, and supporting points of workpieces are identified. Finally, fixture configuration is the final step where fixture components are selected or created and configured to accomplish the locating and/or clamping functions required (Rong and Huang 2005).

The PBP locating methodology was designed with consideration to the design steps and knowledge presented in this subsection. The PBP had to be constrained via fixture components in a fashion that would restrict all but one degrees of freedom (+ z-axis) inside the FDM machines while maintaining the attainable accuracy of the machine, ± 38 μm. The leveling plate fixture for the PBP, workpiece, would be categorized as a dedicated fixture. This is due to the capability of the leveling plate to only constrain a single work piece, the PBP. In the subject of fixture design, the workpiece is typically identified as the object that is being worked on with a certain tool or machine. Although no specific tooling was conducted on the PBP directly when it was placed on the leveling plate fixture, parts were still printed on top of it. As a result, it could still be considered a workpiece, which used a dedicated fixture. Although this is true, the 3D printing technology of the Multi^{3D} system allows for the manufacturing of various product designs, which is not typically a capability of mass production. The PBP workpiece and leveling plate fixture could then be considered to be an exception to this traditional characterization.

Chapter 3

Portable Build Platform and Heated Travel Envelope

3.1 Concept

The concepts of the portable build platform (PBP) and heated travel envelope (HTE) stemmed from the idea of the Multi^{3D} Manufacturing system in general. The goal was to create a novel manufacturing system that has multi-material capabilities and can produce multi-functional (structural parts with electromagnetic and/or electromechanical function, for example) parts. In order to achieve this overarching goal, the PBP and HTE were conceived, which are major components to the successful operation of this system. These components of the system will function to handle and transport the parts developed in the Multi^{3D} system. Figure 3.1 shows the prototype CAD models of these components.

The purpose of the PBP was to be a platform for which the parts can be produced on, similar to the "Platen" of the Fortus 400mc FDM technology developed by Stratasys. The PBP is comparable to the Platen in its ability to grasp a build sheet via vacuum. Although, the PBP differs from the platen in the aspect that it is removable and portable via the MH50 robotic system and is able to locate into each technology of the system. As well, the PBP has the ability to mate with the HTE when they work together to transfer products between stations of the Multi^{3D} system.

The HTE is a forced convection oven with an actuating curtain door. The purpose of this component was to encompass the build area during the transport of the work piece from one system to another in a heated environment to closely replicate the temperatures of the Fortus 400mc's heated envelope when printing with polycarbonate, 145°C. Maintaining the heated environment around these components will mitigate poor filament bond strength, which ultimately effects mechanical properties (Sun, et al. 2008). The HTE was equipped with an actuating door

mechanism allowing the HTE to pass over parts prior to covering them, which as a result increases the build height/volume overall.

The robot end-effector was another component that was conceived and mounted to the end of the MH50 robotic system. The purpose of the end-effector was to grasp and transport the PBP and HTE from station to station of the Multi^{3D} system. The end-effector design used a fork-lift type of beams to lift and sustain the weight of the PBP and HTE. The end-effector design incorporated a pneumatic parallel gripper used to grasp and restrain these components while moving them. The design also incorporated a port for mating with the PBP to supply it with vacuum, -42.3 ±8.5 KPa, for grasping the build sheet, during transport.

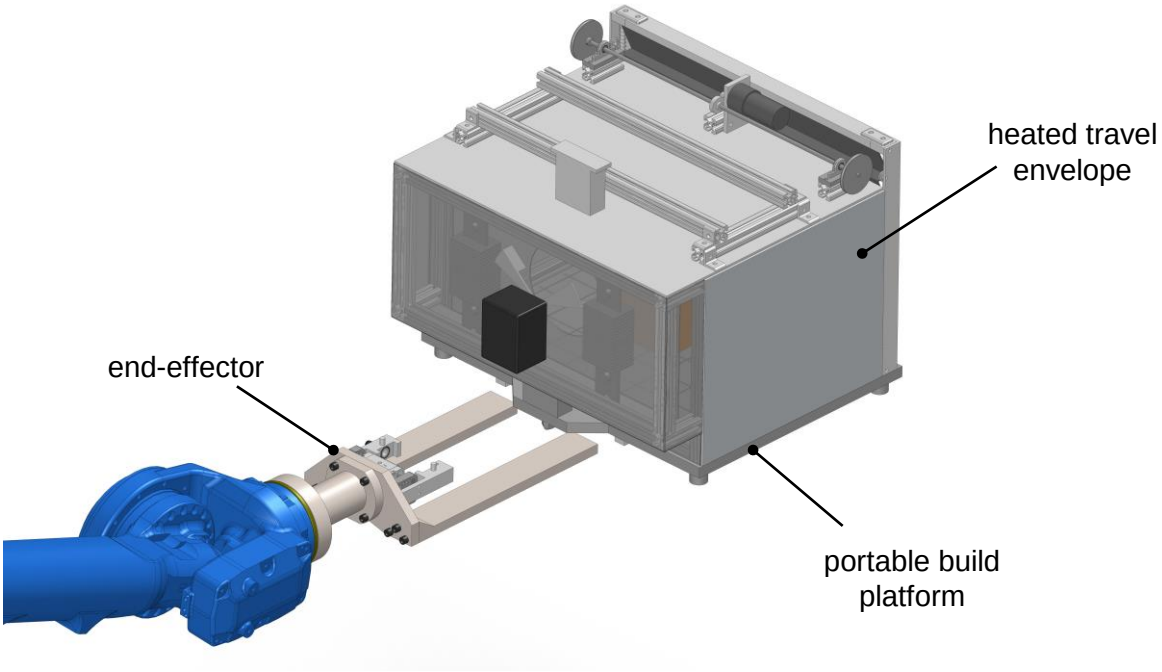

Figure 3.1. SolidWorks CAD models of PBP, HTE, and end-effector prototypes

3.2 Design Objectives

In order to achieve the goal of developing the portable build platform (PBP), heated travel envelope (HTE), and end-effector, the design process was organized into four particular objectives. These objectives were as follow.

(1) Design and develop the PBP with the capabilities of providing a vacuum (-42.3 ±8.5 KPa) for suctioning the required build sheet that parts are printed on and being accurately positioned in all stations of the Multi^{3D} system

(2) Design and develop the HTE with the ability to mate with the PBP, enclose built parts, and maintain a targeted controlled heated environment of 150 °C, 5°C higher than the envelope temperature of the FDM machine when printing with PC

(3) Design and develop the robotic end-effector with the ability to sustain the weight of the PBP and HTE (25.5 kg) and the ability to securely grip these components to reduce movement during transfer processes

(4) Design these components around the appropriate design constraints (dimensional, weight, etc.) and with consideration to expanding the height of the build volume in order to fully utilize the current build capabilities of the FDM printers and to extend those of the Multi^{3D} system

3.3 Design Constraints

The design of the subsystems and structures of the portable build platform (PBP) and heated travel envelope (HTE) were influenced by numerous constraints of the Multi^{3D} system. The FDM printers, CNC router, and Yaskawa MH-50 robot were the most prominent components that guided the designs. Four particular constraint categories of interest included dimensional, weight, temperature, and functionality.

Table 3.1. Dimensional constraints of the PBP and HTE assembly in respect to the technologies within the Multi^{3D} system.

Dimension (axis)	Constraining Components	
	Fortus 400mc	Techno LC 3024
Width (x)	build envelope entrance, 476 mm	N/A
Length (y)	front edge of platen to back wall of build envelope, 403 mm	N/A
Height (z)	z gantry to extrusion tip, 445 mm	overhead gantry, 300 mm

3.3.1 Dimensional constraints

The dimensions of the PBP and HTE were both dictated by constraints of the FDM printers and tabletop CNC of the Multi^{3D} system. The PBP and HTE were anticipated to operate concurrently the majority of the time, which causes them to dimensionally limit each other as well. One of the most important examples of this is how each component limits one another's height. When operating together, their combined height is limited by the dimensions of the Fortus 400mc's envelope. As a result, the dimensional constraints of their "assembly" was important to consider. Table 3.1 indicates the specific constraining criteria for the PBP and HTE assembly. As well, dimensional constraints concerning the end-effector interaction had to be considered. The end-effector needed to be capable of handling the components correctly while they are inside the FDM systems and the CNC router. As a result, the dimensions of the end-effector were taken into consideration

One of the more influential constraining factors considered was the enlargement of the build volume. Achieving the largest build volume, specifically through height, while considering other constraining factors of the Multi^{3D} was essential to fully utilize the current capabilities of the

FDM printers and as well to extend the capabilities of the overall system. To work towards this objective, the concept of using an actuating door on the HTE was conceived.

3.3.2 Weight constraints

The weight of the designed constituents was dictated by the capabilities of the Yaskawa MH-50 Motoman assembly robot. The payload of the MH-50 is rated at 50 kg (110.3 lb.). The weight constraint directly influenced the material selection of the components used in the designs. Specifically, the use of aluminum 6061 and various steels (SS 304, 1018, etc.) was considered and CAD software (SolidWorks) was utilized in weight estimation of certain components. As well, the weight of the end-effector had to be of major consideration as it was made of SS304, a stronger yet heavier material in comparison to aluminum, in order to sustain the weight of the PBP and HTE during their transport.

3.3.3 Temperature constraints

The material and component selection for the PBP, HTE, and end-effector was constrained to the temperatures they were expected to experience during the processes of the Multi^{3D} system. The FDM envelope temperature reaches 145°C when printing with polycarbonate material. As a result, a 150°C value was used as a base line for the temperature capabilities of the material and components selected for design of the material handling prototypes.

3.3.4 Functionality

Sustaining a heated environment around the printed parts was essential to mitigate poor filament bond strength (Sun, et al. 2008). The enclosure was heated through the use of forced convection and heating elements. The addition of an actuating door was necessary to increase the build height. The door allowed the HTE to slide over the part when inside the Fortus 400mc or while on the table top CNC or any other station of the system. A vacuum system that allowed the

PBP to be portable was required to secure the build sheets used in the current Fortus 400mc build process. A method of supplying the required vacuum at all times, within the stations and while transporting was a necessary function.

3.4 Prototype Design

3.4.1 Portable Build Platform

The concept design of the PBP (Figure 3.2) was shaped around the design of the Fortus 400mc's build platform, otherwise known as the platen. The key features of the platen that were incorporated into the PBP design include the center vacuum port, the vacuum channels, and its base material. The structure of the PBP was made from 6061 aluminum to allow the platform to be light weight. The dimensions of the design were shaped in respect to the constraints previously discussed. New design features that were integrated include the outer rim for the HTE attachment,

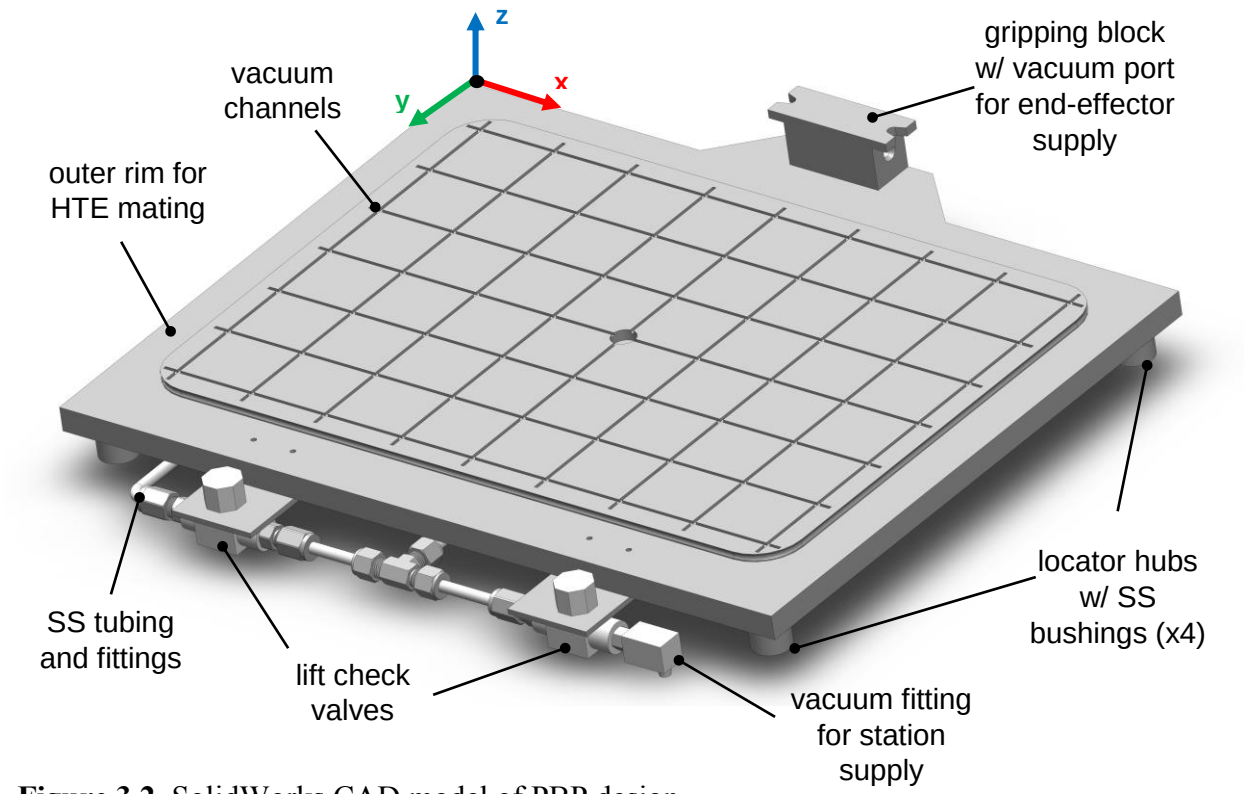

Figure 3.2. SolidWorks CAD model of PBP design

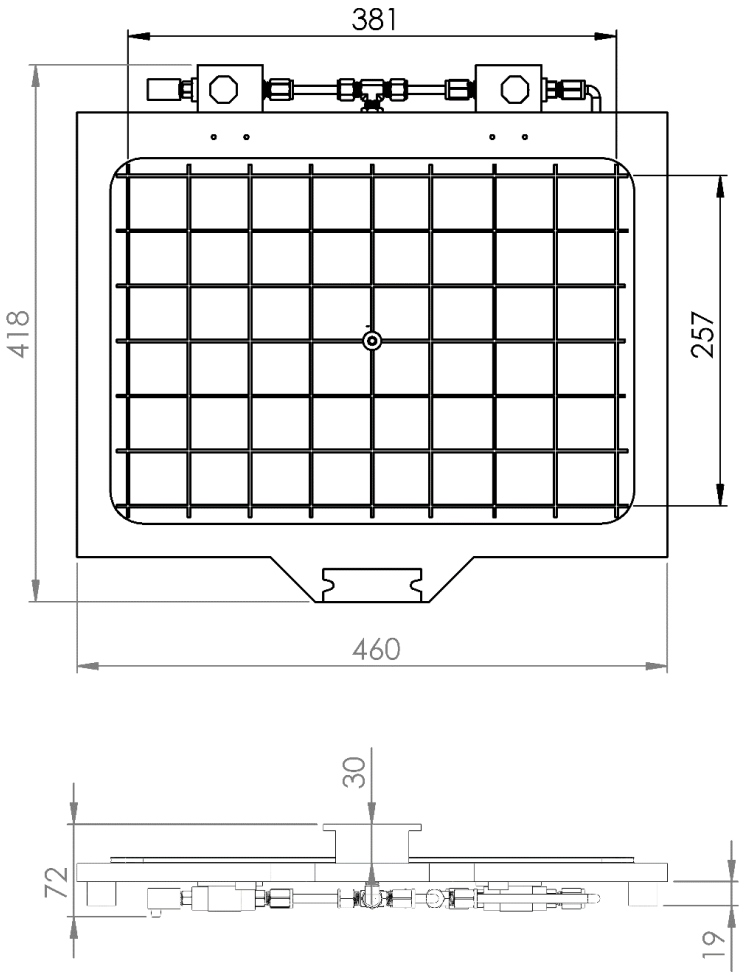

Figure 3.3. Overall dimensions and build area dimensions of PBP (top and front views)

the gripping block for interaction with the material handling robot, and the locator hubs. The outer rim is a flat surface on the edges of the PBP, which is reserved as area for the HTE to sit on. The gripping block served two main functions, to properly locate the end-effector and supply vacuum via the end-effector. The width and length of the PBP build area were reduced to 257 mm by 381 mm (10-1/8" x 15") in comparison to the platen which has a build area of 355 mm by 406 mm (14"x 16") (Figure 3.3). The weight of the prototype was measured to be approximately 8.8 kg.

3.4.1.1 Locator pins and gripping block

The methodology integrated into the design of the locating scheme of the PBP is the use of the locating pins, concentric locators, and bottom locating (Rong and Huang 2005). The

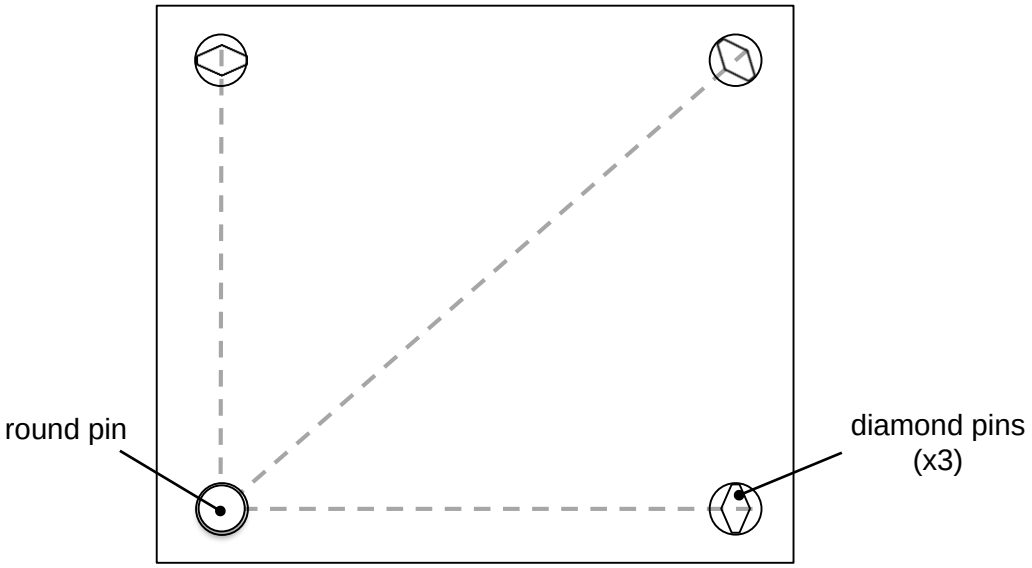

Figure 3.4. Locating pin placement and orientation

concentric locators can produce accurate locating by restricting 11 out of 12 degrees of freedom, the positive z axis being the only free axis. Bottom locating was necessary to allow the PBP to be removable from the system. To maintain the achievable accuracy of the FDM printers, ±38 μm, tolerance within this range between the diameters of the pins and concentric placements was necessary, but can cause binding from the tight interfacing. The use of one cylindrical pin and 3 diamond pins is used to reduce binding (Figure 3.4.). The diamond pins will only contact at two smaller radial faces, which will reduce the binding. The contact surface area in a circular pin is estimated at 319 mm^2 and in a diamond pin at 68.8 mm^2, which is 78% less contact area. The binding is also minimized by orienting the diamond pins in a fashion where they "point" to the round pin, as seen in Figure 3.4 (Rong and Huang 2005). The difference in diameters of the concentric placement holes and the pins chosen was approximately 0.02 mm.

The fourth locator, directly diagonal to the round locator was removed from the locating scheme in order to not over constrain the PBP. The vacuum fitting was required to mate with the appropriate vacuum port in the area where the fourth pin was originally located, as a result becoming another constraint to PBP. This was another reason the fourth pin was excluded from

the locating scheme. It is also of importance to mention that other locational aids were considered when developing the locating methodology. The particular constraining criteria that limited the locational aids that could be utilized was the elevated temperatures. Clamping mechanisms could also have been employed into the locating methodology, but would require actuators. High temperature environments, up to 150 °C in this case, are not ideal for the proper operation of typical pneumatic and electrical actuators (Bar-Cohen 2014).

The leveling plate, seen in Figure 3.5, was a component designed to be mounted inside a Fortus 400mc printer to the beams of its z-gantry. The leveling plate was used to locate the PBP inside the printer via the previously discussed locating pins. The positions of the locating pins are adjustable. The leveling plate used manually adjustable pins (threaded set pins) under its structure to level the x-y plane of the PBP relative to the x-y motion of the Fortus 400mc extrusion head. The plate also contained a vacuum port for mating to the fitting on the PBP (discussed further in section 3.3.1.2). The fourth locating pin was excluded from the design, as previously mentioned. The leveling plate structure was made of 1018 low carbon steel in order to ensure it is a rigid structure for the PBP and, at times, the HTE to sit on. The stiffness of the leveling plate is crucial to maintaining accuracy of produced parts, as any extent of deformation in its structure can have possible implications to locating accuracy. The full design process utilized in the development of the leveling plate is not discussed in detail in this document, only the most important design features are discussed which pertain to its development in consideration to the locating of the PBP on top of its structure.

The PBP was designed with four hollow cylindrical hubs on its bottom surface which were used for mating with locating pins. The hubs contained hardened steel bushings which were press-fit into the inner portion of the hubs and were held by a set screw. The interference between the

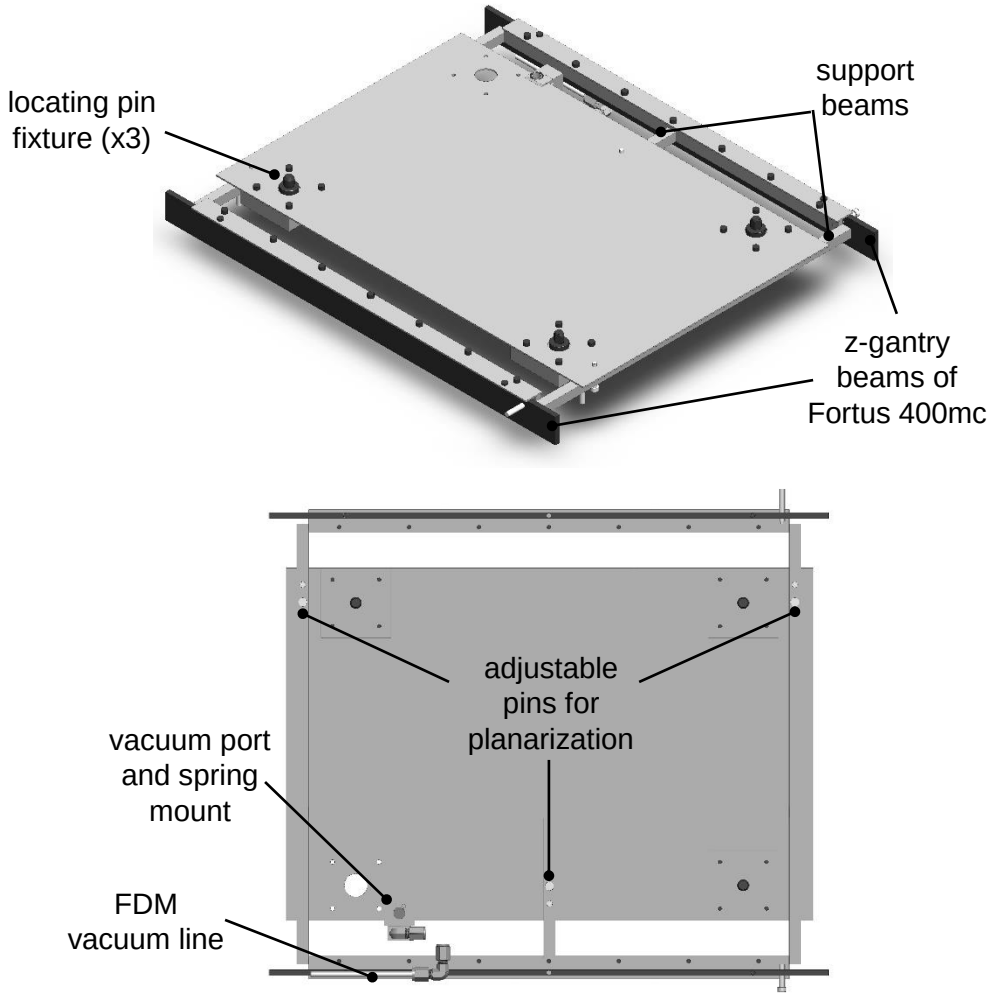

Figure 3.5. Leveling plate CAD model, design features

inner diameter of the hub and outer diameter of the bushing was 0.01 mm for press-fitting. The bushings were intended to constantly interface with the surface of locating pins, made of hardened steel, when the PBP is deposited in and removed from the various stations. The hubs alone are made of 6061 aluminum, the PBP base material. The constant contact of aluminum and steel surfaces would wear out the aluminum of the hubs, eventually leading to inaccuracies while locating because of the lost material on the hub's surfaces. The stainless steel bushings were less prone to wear during this contact, which was the main purpose of including the bushings into the design. Set screws (size: 4-40), threaded on the side wall of the hubs, hold the bushings in place during thermal expansion (Figure 3.6.).

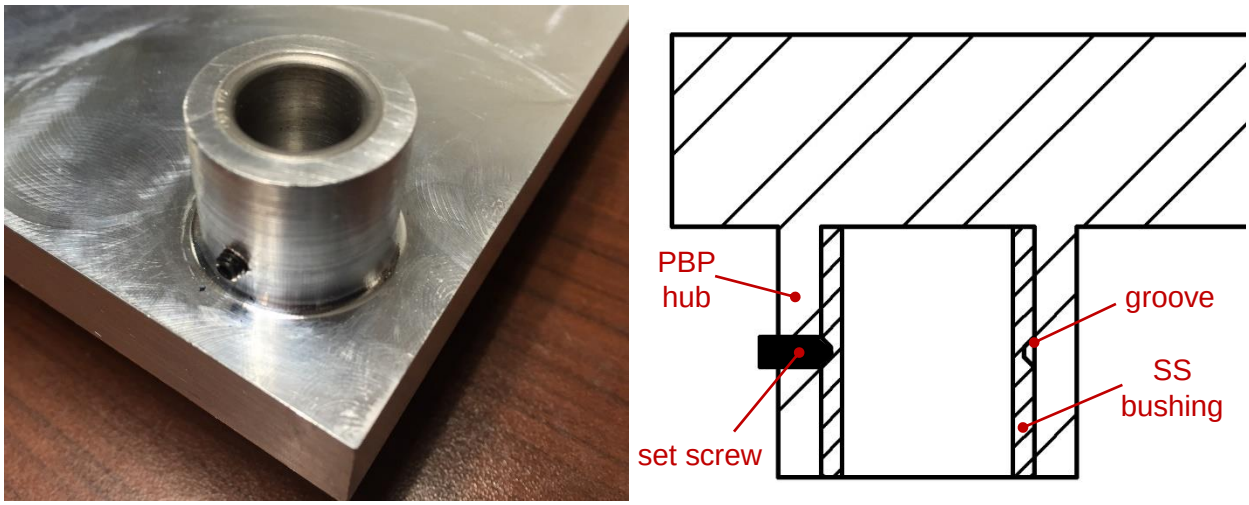

Figure 3.6. Photograph of PBP hub with bushing with set screw and sectioned drawing of design

$$r_f = r_i(1 + \alpha \cdot \Delta T) \qquad \text{[Eqn. 1]}$$

Table 3.2. Thermal expansion calculations for PBP hubs and SS bushings

ΔT	R (m)	r (m)	α (m/C*m)	Rf	rf
125	0.022225	0.015875	2.52E-05	0.022295009	0.01592501
125	0.015875	0.0127	1.08E-05	0.015896352	0.01271708

The hubs of the PBP, made of 6061 aluminum, are expected to expand at a faster rate relative to the SS and hardened steel when exposed to the envelope temperatures of Fortus 400mc systems. The thermal expansion of the hubs and bushings was calculated via thermal expansion equation, Equation 1, based on temperature change (Cengel and Ghajar 2011). The expansion of the outer (R) and inner radiuses (r) of the hubs and bushings were calculated for the same temperature change from 25 °C to 145°C. The dimensions and thermal expansion values (MatWeb, LLC 2015) used for the calculations and final results are shown in Table 3.2. The expansion creates a gap of approximately 28 µm (0.001") between the bushings and hubs of the design. This gap, which would allow movement of the bushing, would potentially effect accuracy. As a result, the set screws were included in the design to restrict movement of the bushings during expansion.

The gripping block of the PBP served two main functions during transportation via the end-effector of the MH-50. One function consisted of the gripping block's use to provide the necessary vacuum through a side port that mates with the end-effector. The gripping block has an internal 90 degree channel that connects its side port to the base of the PBP (Figure 3.7.) The gripping block was a separate piece of the PBP and mounts via four threaded holes. As a result, a groove for a high temperature Kalrez 4079 O-ring was added between the mating surfaces of the PBP and gripping block to prevent air leaks. The function of supplying vacuum will be further discussed in the next subsection, 3.4.1.2. The other function of the gripping block involved its use as a locating criteria for the end-effector when initially gripping the platform. This also included its function in preventing x-y plane movement of the PBP when being transported. Locating pins, part of the clamps of the end-effector (see subsection 3.4.3), fit into to the top edge grooves of the gripping block, which restricts the x-y plane movement partially.

Aluminum rectangular alignment bars were mounted beneath the PBP that mate closely, approximately 1.5 mm tolerance, to the outer edges of the end-effector's forks and are used to further restrict x axis movement of the PBP (Figure 3.8.). This mating was not considered to be as critical and as a result the tolerance between the bars and forks was larger. As well, larger tolerance was required in order to aviod collision or frictional forces when the end-effector attempted to

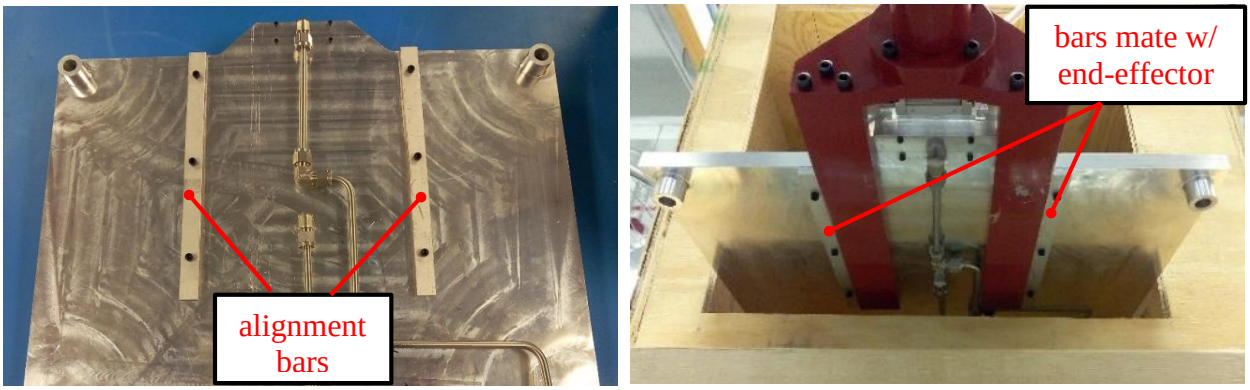

Figure 3.8. Photos of alignment bars of the PBP

mate with the PBP. The main purpose of the bars were to reduce x-y plane movement without over constraining the PBP on the end-effectors prior to depostion.

3.4.1.2 Vacuum system

The vacuum system was designed to function with two supply sources. The first supply source coming from the station of the Multi^{3D} system that the PBP resides within. The second supply source coming from the end-effector, which is utilized to maintain the vacuum when transporting the PBP. The system incorporated two lift check valves which were used to restrict air flow to a single direction. These were necessary to avoid unwanted pressure change when transitioning between vacuum sources and when one of the supply inputs is unused. The vacuum system was composed of SS tubing and fittings and was located underneath the PBP (Figure 3.9.).

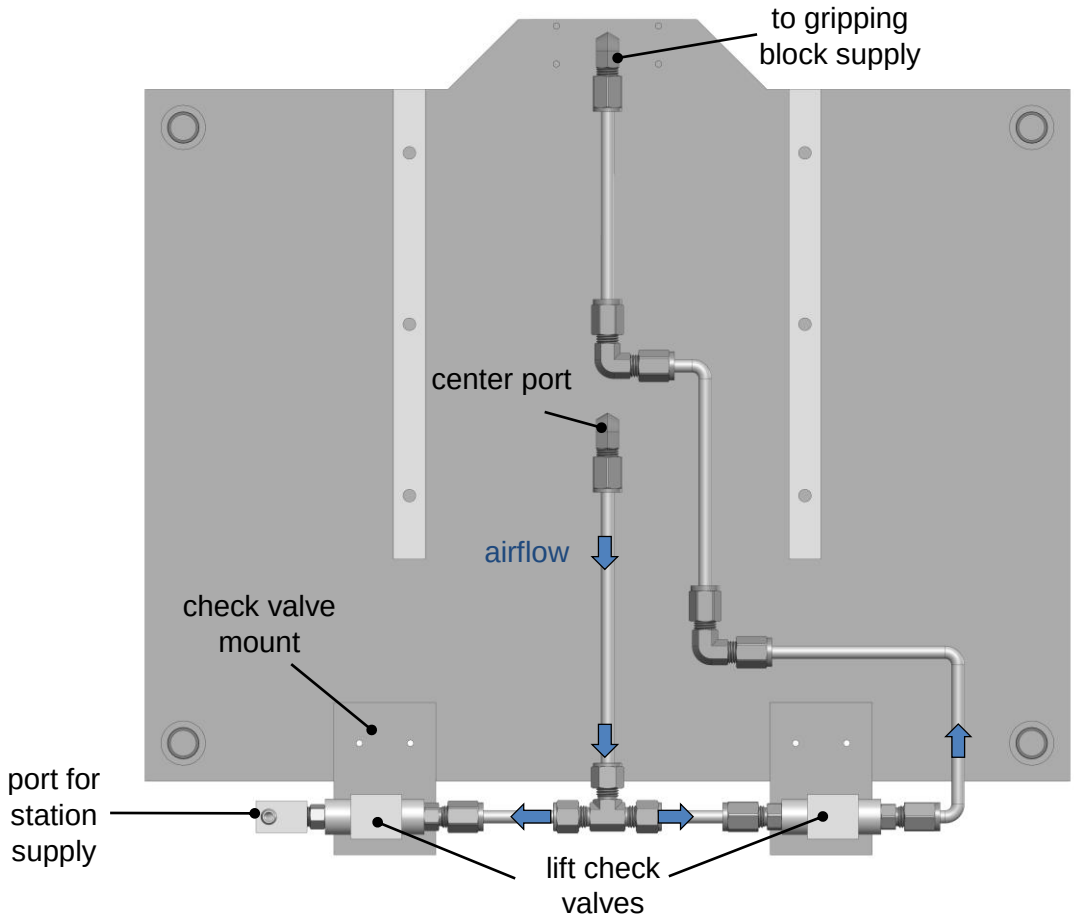

Figure 3.9. Schematic of PBP vacuum system, bottom view of PBP

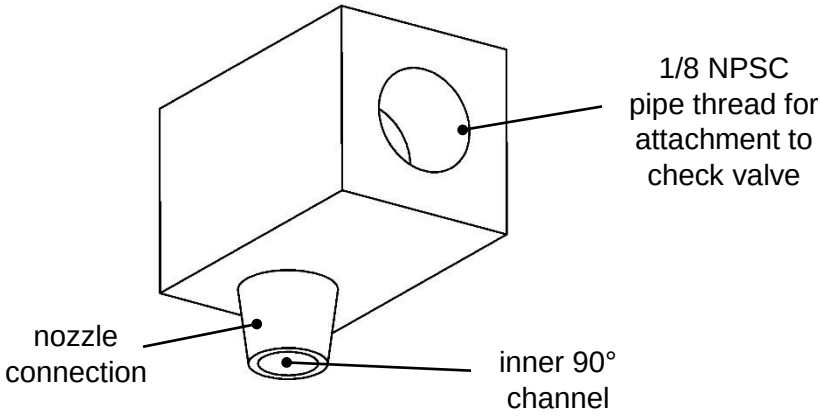

Figure 3.10. Vacuum fitting design features

The check valves are mounted to the back edge of the PBP because they are unable to fit below PBP in the required orientation.

A "vacuum fitting" was attached to the left side check valve to allow mating with a vacuum supply via the appropriate station. The vacuum fitting mates on the leveling plate of the Fortus 400mc via a vacuum port. The vacuum fitting has a cone shape which inserted into and coupled with the vacuum port (Figure 3.10). The vacuum port mount uses a spring mechanism, as seen in Figure 3.11, which gave the component limited vertical motion of approximately 1.27 cm (0.5").

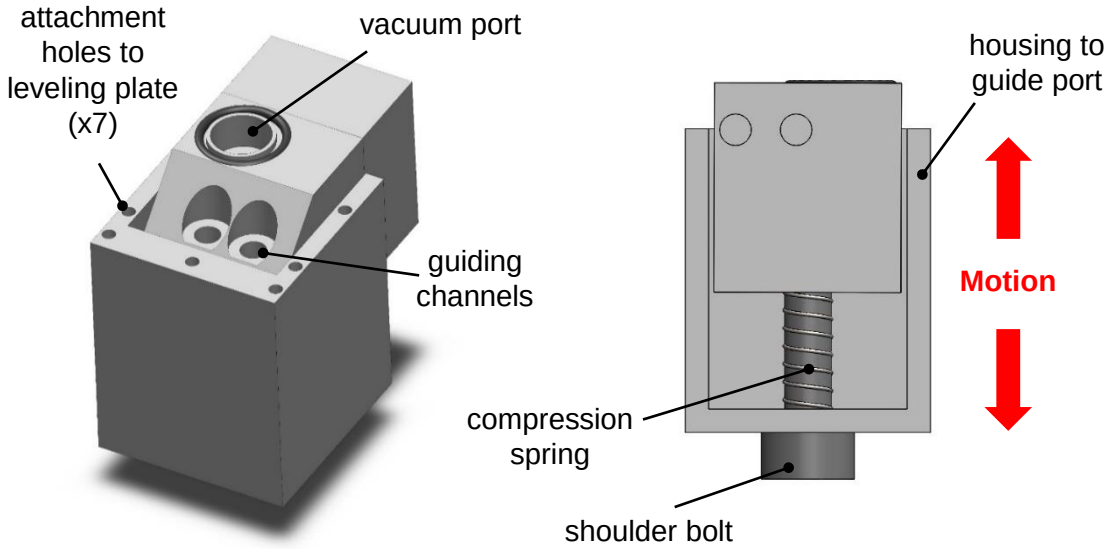

Figure 3.11. Vacuum port mount and spring mechanism design (isometric and back views)

The purpose of the spring mechanism is to improve the mating between the vacuum port and the vacuum fitting on the PBP. The vacuum port was guided in its vertical motion via its mount/housing and shoulder bolts that mate with its guide channels.

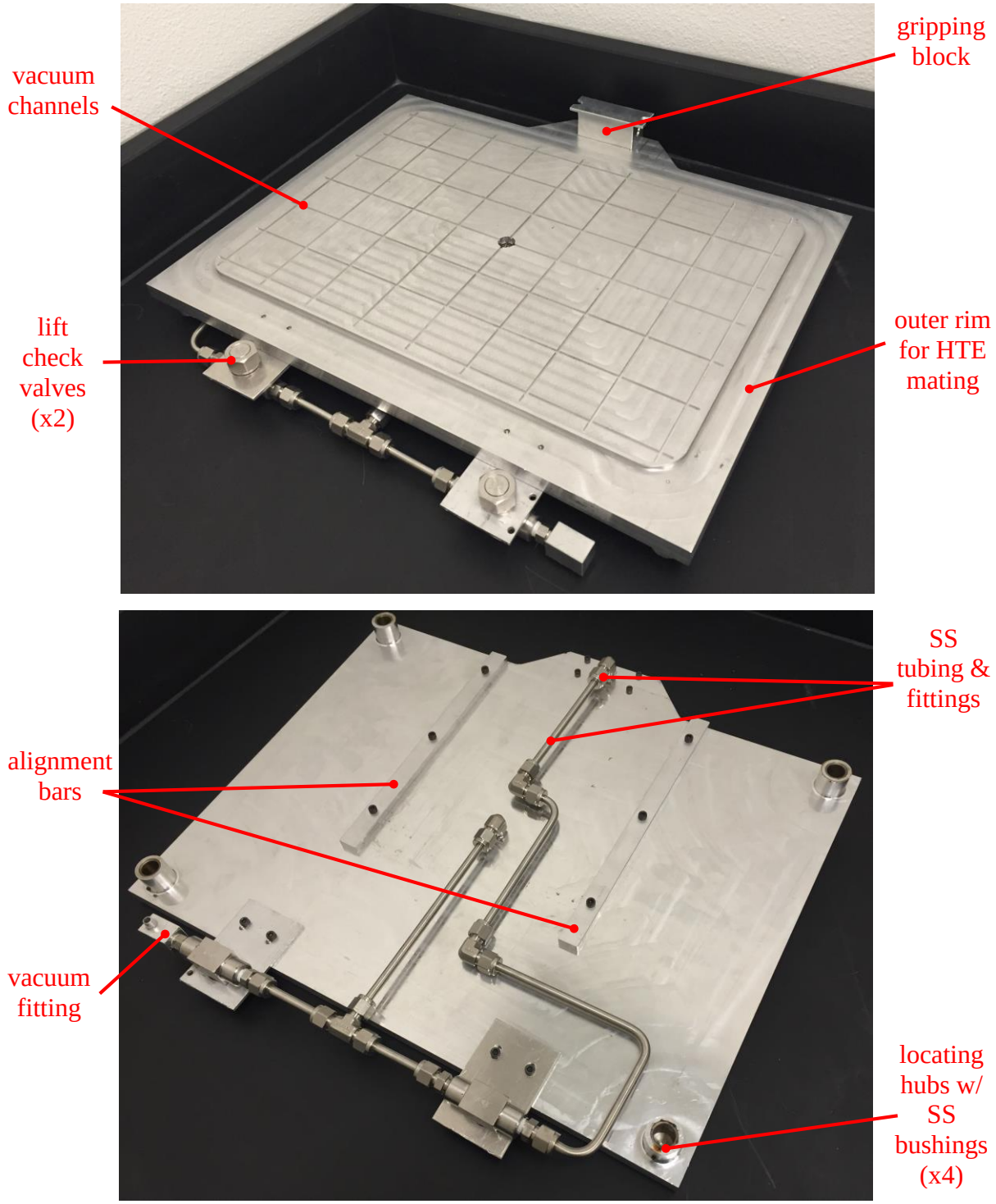

Figure 3.12. Photograph of PBP, top and bottom views

3.4.2 Heated Travel Envelope

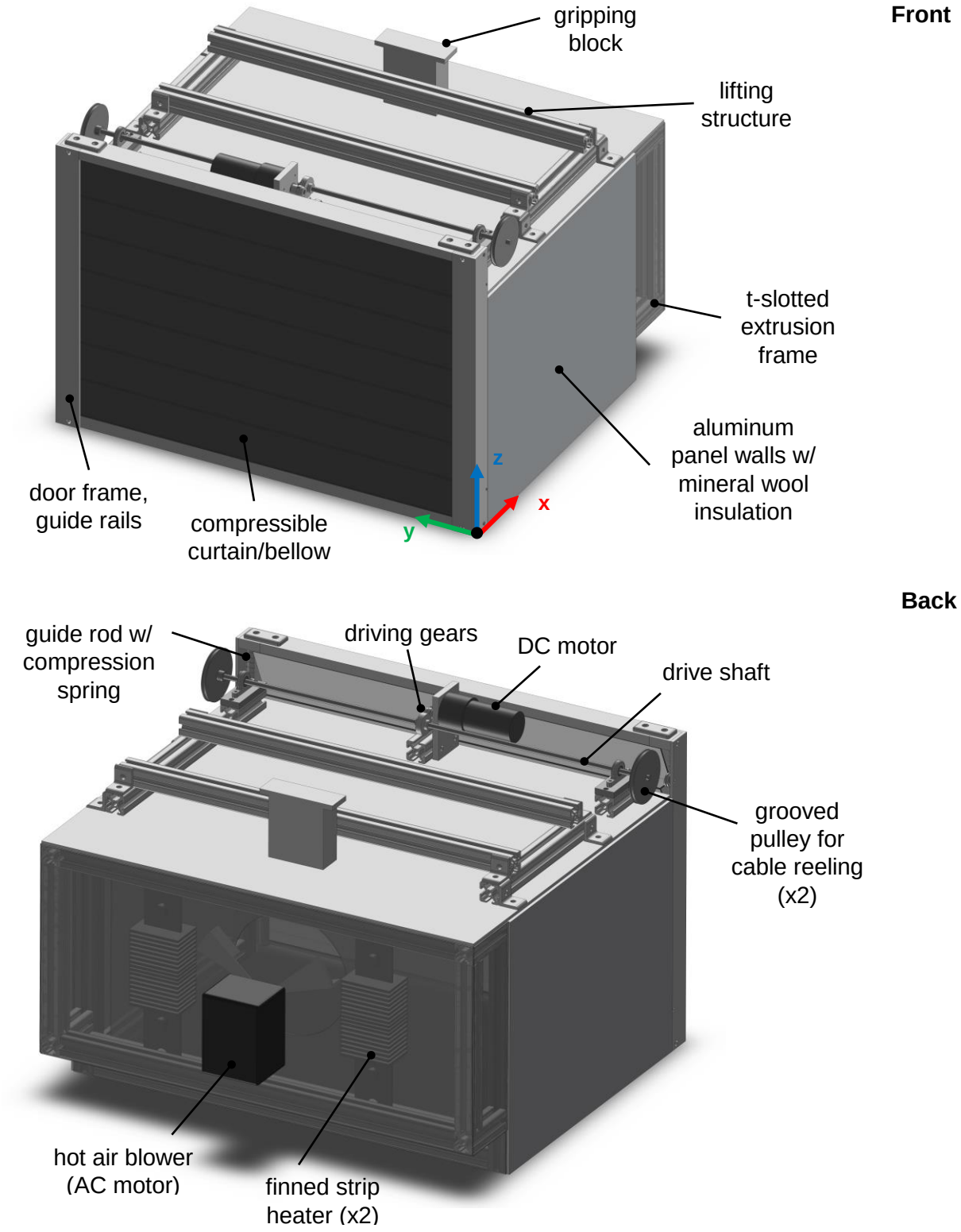

Figure 3.13. SolidWorks CAD model of HTE

The frame of the HTE was assembled from t-slotted 6061 aluminum extrusions. The t-slotted extrusions allowed the frame to be easily customizable when implementing the details of the design. This included the addition of the mineral wool insulation inside the aluminum paneled walls. As seen in Figure 3.13, on the top surface of the HTE, a gripping block and lifting structure are mounted. The gripping block of the HTE served a similar purpose to gripping block of the PBP, excluding the vacuum capabilities which are not necessary when transporting the HTE alone. The lifting structure was directly mounted to the frame and was used by the end-effector to lift and sustain the weight of the HTE (Figure 3.13). The weight of the prototype of the HTE was measured to be approximately 16.8 kg.

3.4.2.1 Convective heating system

The convective heat system of the HTE used a single hot air blower (AC motor) rated to create airflow up to 200 m^3/hr., with a bearing operating temperature of 120°C. The hot air blower was mounted to the back wall of the HTE and has its shaft running through the wall. A shaft extension was manufactured and added to the motor which allows it to fully pass though the thickness (~26 mm) of the insulated wall. It was inherit that the back wall contained insulation in order to isolate the motor, its bearings specifically, from the temperatures of the HTE's interior. A hollow cylindrical tube was added inside the back wall, around and concentric to the shaft of the blower. This cylindrical tube was used to isolate the shaft motor from directly contacting the mineral wool insulation, which could tangle with the shaft and cause damage to the motor. The hot air blower used a 12.2 cm (4-13/16”) diameter and 2.86 cm (1-1/8”) thick blower wheel (centrifugal fan) to circulate the air within the envelope. The fan intakes air through its front center and circulates air centrifugally along its circumference.

The convective heat system used two 400 Watt, 120 V, ceramic insulated finned strip heaters to continuously heat the circulated air. Approximating the area of the "ducts" around the blower wheel to about 5,967 mm^2, the velocity of air flow was approximated at 22.09 m/min. The finned heaters are capable of creating air temperatures between 93 to 204°C with air flow between 15.24 m/min and 30.48 m/min depending on the control scheme. The air circulated by the blower wheel passes through the fins of the two heaters, then vents almost immediately and recirculates through the HTE interior (Figure 3.14). An aluminum panel with a large circular cut out was located in front of the blower wheel and heaters. The panel was used to create "ducts" on left and right sides that direct the air over the heaters and the circular cut out allows the blower wheel to intake air. The walls of the HTE contain mineral wool insulation rated for temperatures up to 650 °C with a K factor (thermal conductivity) of 0.033 W/m-°K.

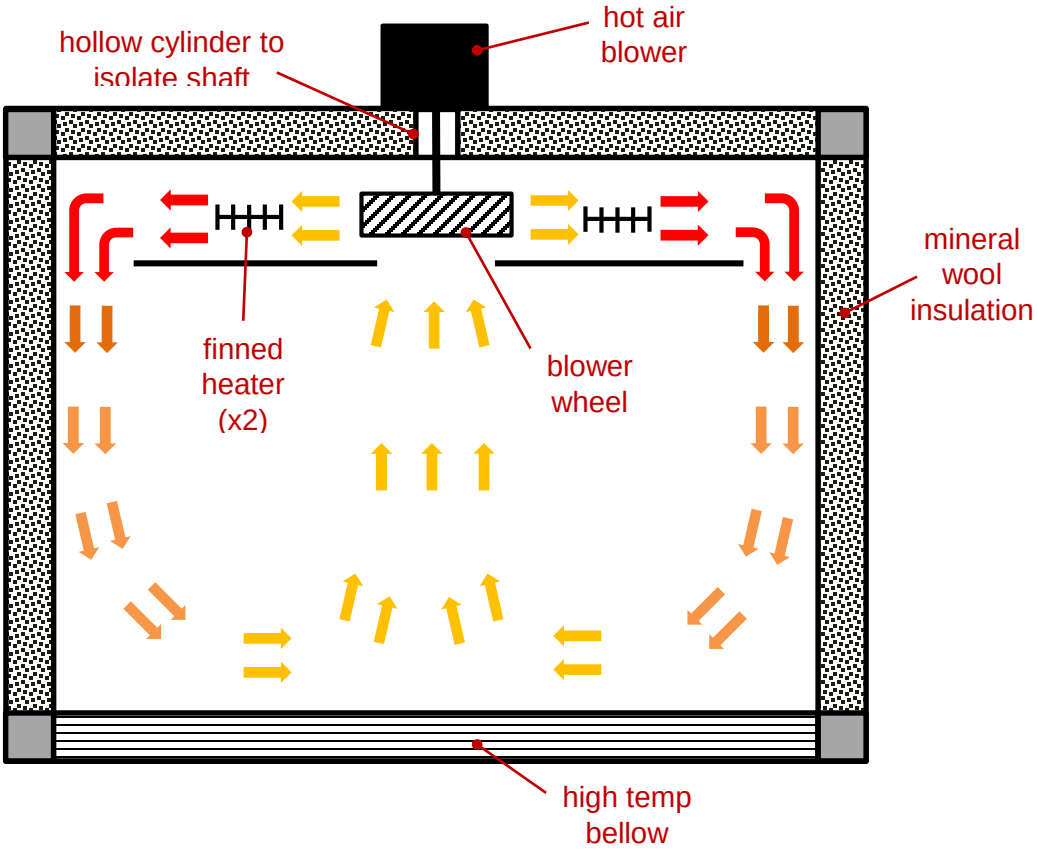

Figure 3.14. Diagram of convective heating methodology for HTE

The HTE heating system was controlled by a CNi16D44-EIT PID temperature controller and two SSR330DC10 solid state relays (Omega Engineering INC, Stamford, Connecticut). The temperature controller pulses (small bursts of current) the solid state relays with 5 VDC which controls the AC inputs to the strip heaters. The PID settings control the pulsing to actively control the relays and regulate the power input to the heaters which worked to closely achieve the target temperature. The heaters were wired inside the HTE with 14 AWG PTFE and fiber glass insulted wire. A K-type thermocouple probe is mounted in front of the left side vent of the heating system (Figure 3.15). The thermocouple was used by the temperature controller to monitor the temperature of the air. The wiring inside of the HTE was channeled outside to exterior via an eight multi-conductor feed through, to ensure no heat loss. Six of the eight feed through holes are used in the current design for the heaters and thermocouple wiring. Power connectors are used to connect the internal wiring to 7.62 m (25 ft.) extension cables which allow the HTE to move around freely from station to station of the Multi^{3D} system while still receiving power. The HTE was capable of reaching an internal temperature of 150°C in approximately 30 min, with an approximate ± 8 °C fluctuation.

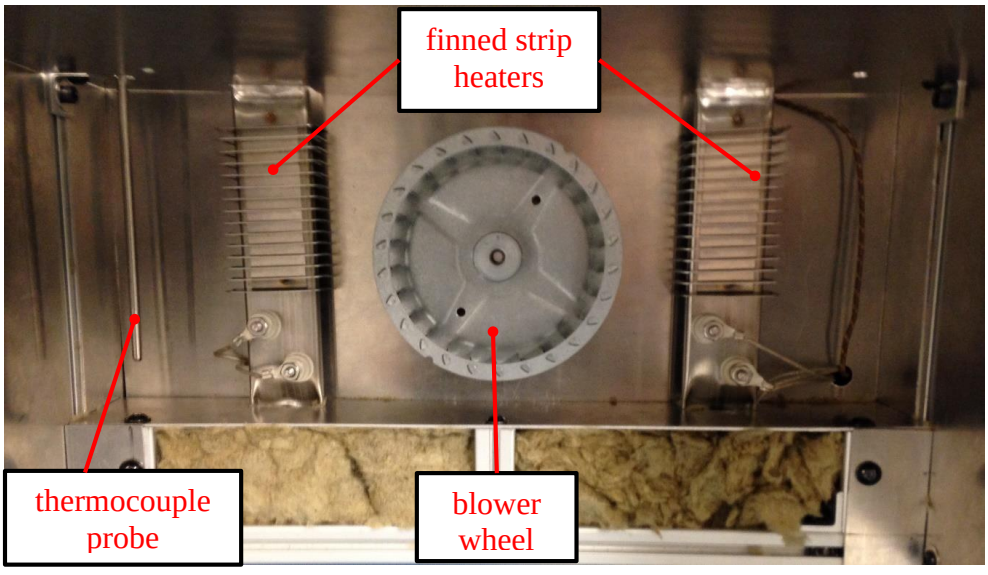

Figure 3.15. Inside of back wall of HTE, convective heating system with blower and heaters

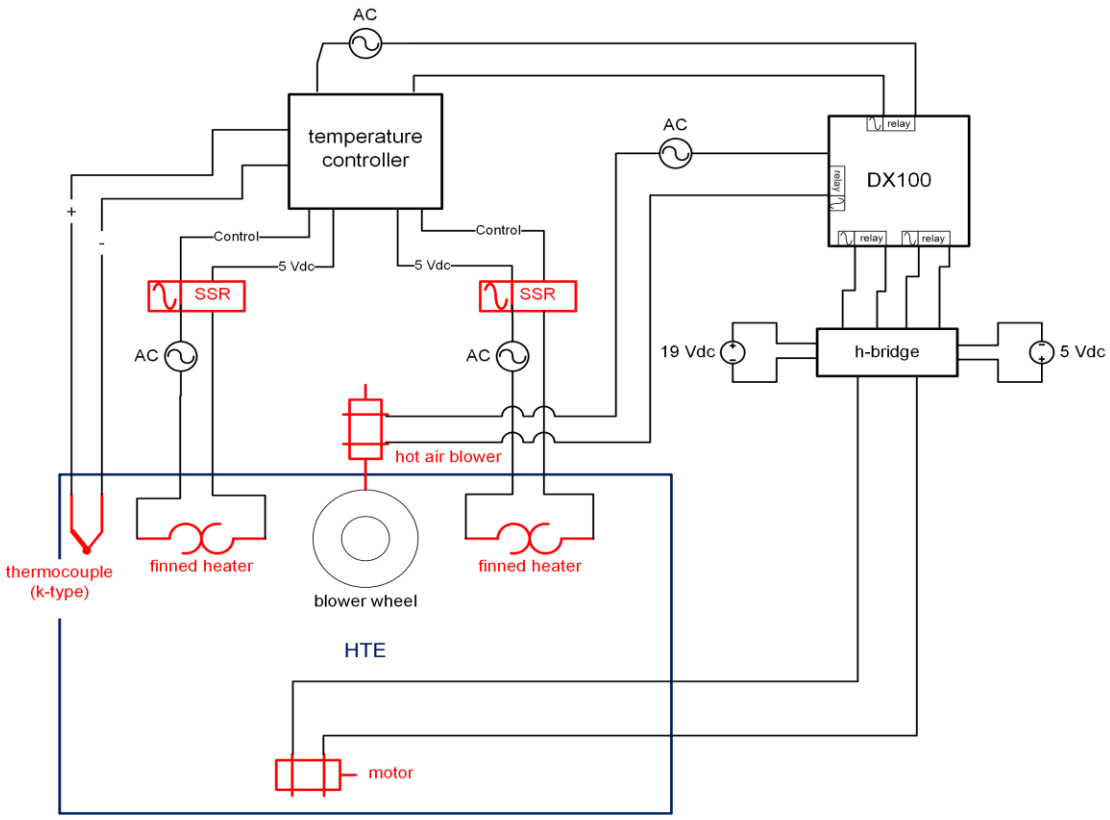

Figure 3.16. Electrical wiring diagram of HTE

The DX100 controller of the MH50 robot was used to control the robot's motions via LabVIEW. A wide variety of components of the Multi^{3D} system are controlled by the DX100 other than the robot. With the current setup, the HTE heating system is controlled via an AC power strip, but it is possible to control the system with the DX100. Figure 3.16 shows the wiring setup designed for control via the temperature controller and the DX100. This includes the wiring of the motor for the actuating door of the HTE.

3.4.2.2 Actuating curtain door

The HTE used an actuating curtain door to increase the height (~22 cm) of builds within the Multi^{3D} system. The design of this actuating door included a high temperature (fiber glass, Teflon) compressible bellow/curtain attached to flexible SS cabling. The cabling attached to both ends (length wise) an aluminum L-shaped extrusion, which is the base of the door. The cables

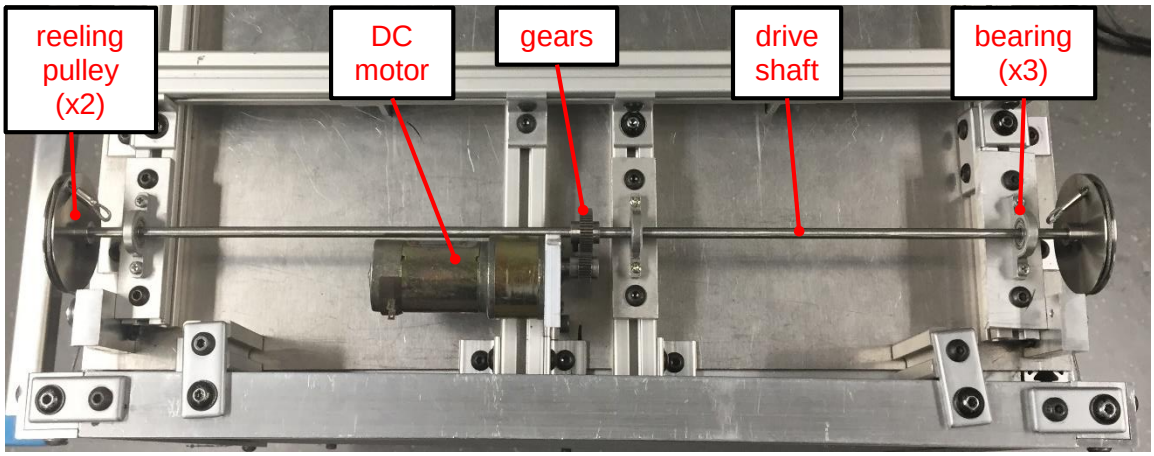

Figure 3.17. Cabling reeling system of actuating curtain door

were guided by two pulleys and reeled onto a large grooved pulley by a DC motor. The reeling pulleys were controlled by DC motor via two gears that rotate a drive shaft (Figure 3.17). Based mounted bearings are used to support and mount the drive shaft in the appropriate locations. The closing mechanism worked via a compression spring that decompresses and assists the door to close when the motor reversed (Figure 3.18). This ensured smooth closing of the door after the actuators retract. The springs were 29.2 cm (11.5”) in length and were located around two guide rods that were located on both ends of the curtain. The door base had two holes on its ends, containing sleeve bearings, which were directed by the guide rods. The springs used were chosen based on their ability to compress to 3.8 cm (1.5”), which was required for the curtain to compress to the ideal amount, approximately 25.4 cm (10”). The force required for full deflection of the spring was rated at 3.29 N (F_s).

The DC motor was rated at a peak torque of 24.5 N-cm (557 oz.-in). The torque required for the full function of the door was calculated with simple torque equations based on the weight of the curtain door’s aluminum base. Free body diagrams were created to illustrate the gear and pulley systems loading scenarios (Figure 3.19) (Close, Fredrick and Newell 2002). The ball-bearing pulleys used to guide the cables to the base of the door were considered to be ideal (i.e.,

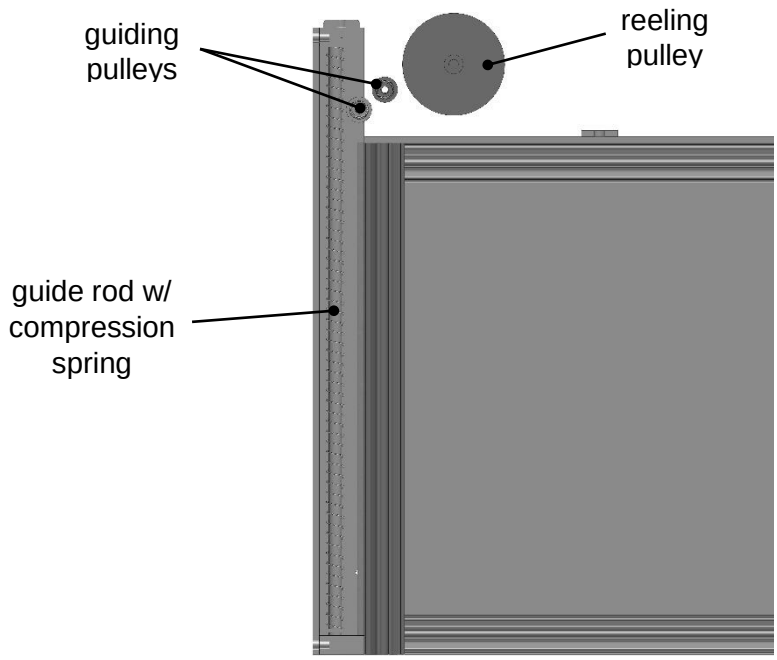

Figure 3.18. Section view of the actuating door system, spring and pulleys

not causing any friction/reaction torques). This assumption included the support bearings used for the drive shaft. The gear teeth ratios of the drive gears were also taken into consideration for the calculations (n_1=30, n_2=50).

$$\frac{T_2}{T_1} = \frac{n_1}{n_2} \quad \text{[Eqn. 2]}$$

$$T = F \cdot r \quad \text{[Eqn. 3]}$$

Equation 2 was used to calculate the torque required to compress the curtain and lift the curtain base, whose mass was approximated to 0.39 kg, based on the weight of the aluminum base (w = 0.55 N) and compression force of the spring (F_s=3.29 N). The radius of the pulley used to reel the cable was 5.08 cm (2.00", r_p) which resulted in a torque of 19.5 N-cm (T_p) required to actuate the door. The torque of the pinion gear (smaller gear, T_1) was given by the rated torque of the motor, since it was directly mounted to the shaft of the motor. The torque transmitted to the

larger gear, the drive shaft and to the cable reeling pulley (T_2) was calculated by Equation 3 using the ratio in gear teeth (n_2/n_1). The torque was calculated to be 655 N-cm.

Although the calculations point to an unnecessary amount of torque used for the system than required (i.e., over designed), the required torque was not the main concern during component selection of the actuating system. The rated torque of the motor selected was large enough to have flexibility with the additional components used for the system. The components were selected based on different needs of the system. The reeling pulley was selected based on a circumference and outer groove depth combination (2" & 1/16") that would be capable of reeling the required amount of cable. The gears used in the design were mainly incorporated as a form of power transmission to the drive shaft. The gear ratio between the two was arbitrarily chosen to increase the torque outputted in order to compensate for frictions not considered in the calculations. The calculations of torque were done mainly to verify the torque would be sufficient for the system to function with the selected components.

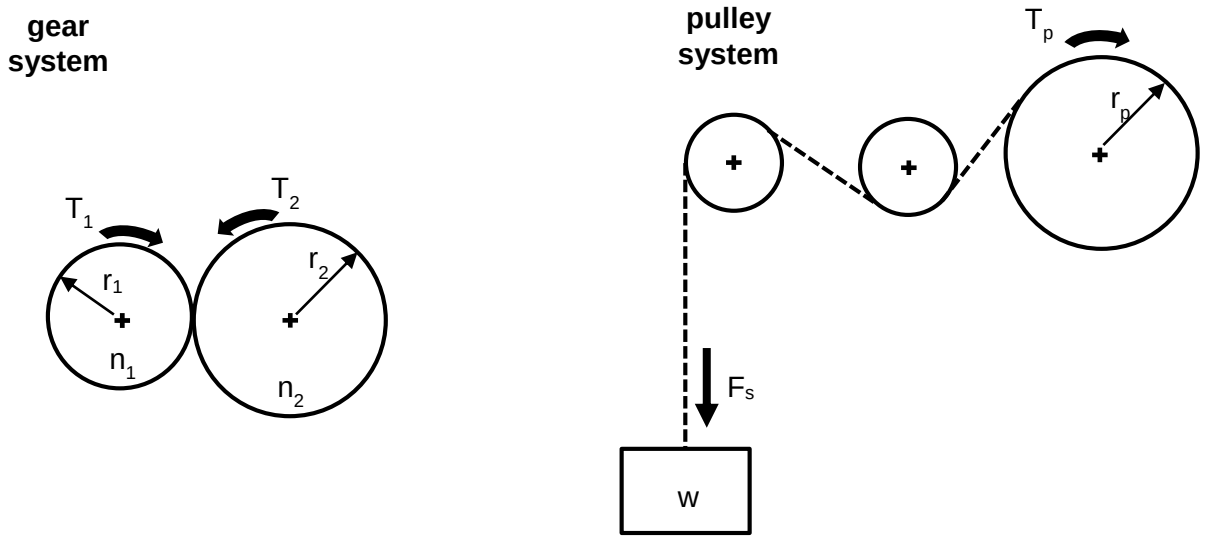

Figure 3.19. Free body diagrams of gear and pulley systems

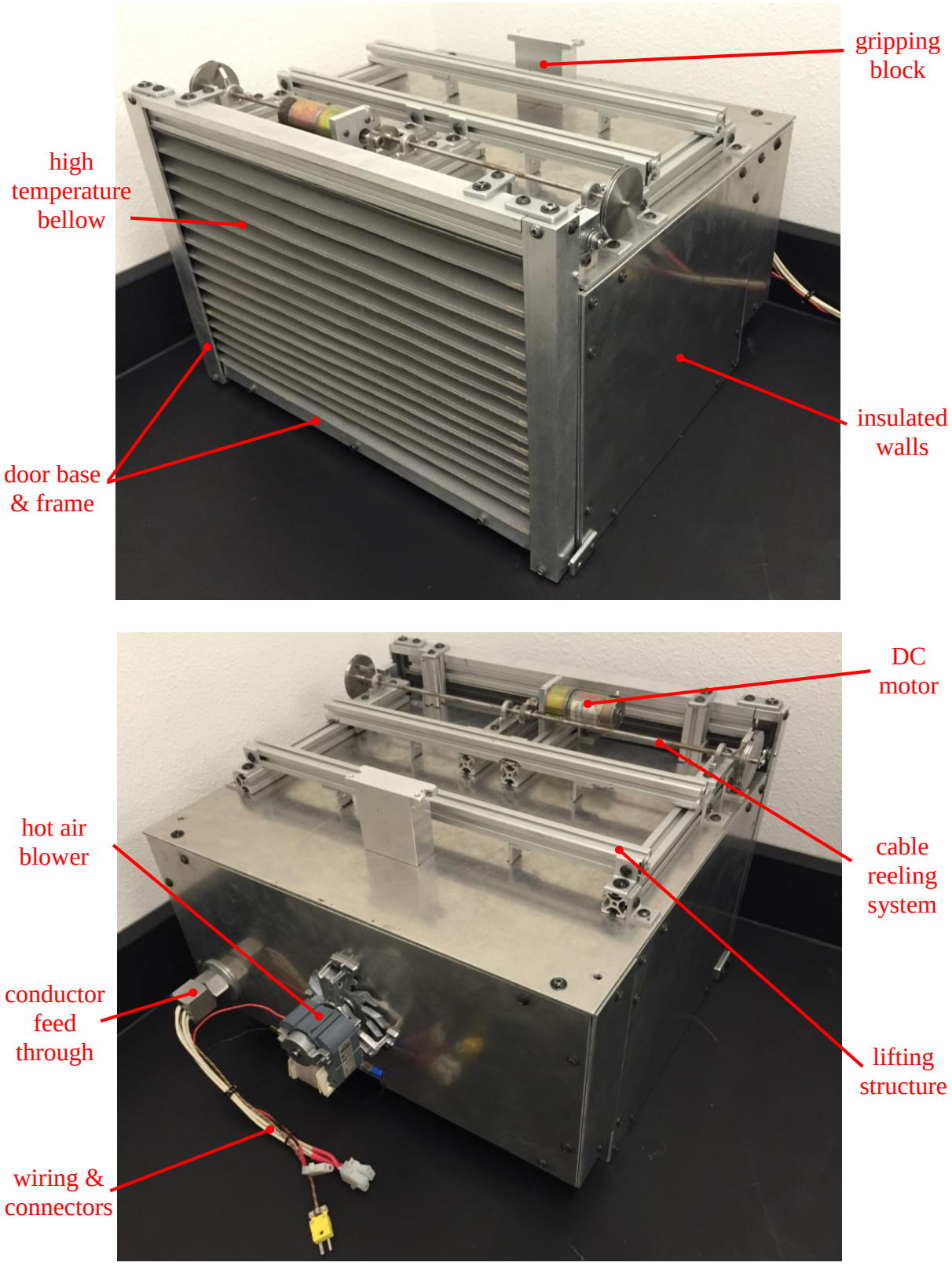

Figure 3.20. Final prototype of HTE, front and back views

3.4.3 Robot end-effector

The robot end-effector was designed to lift, grip, and sustain the weight of the PBP and HTE assembly (Figure 3.21). The payload it was designed to sustain was 41.8 kg, the remainder of the MH50 payload (50.0 kg) excluding the weight of the end-effector (9.2 kg). The end-effector was able to lift these components individually or together via forklift type beams. It gripped the components via c-clamps and a pneumatic parallel gripper at the component's gripping block. The end-effector was able to supply vacuum to the PBP at its gripping block via a port designed into the left clamp

The clamps were directly attached to the parallel actuator via through holes and M4 bolts. The clamps were designed in a "c" shape in order to wrap and grip the vertical surfaces of the gripping blocks. The left clamp has a through hole in the center of its c-shape which was used to channel air at the gripping block for supplying the vacuum as seen in Figure 3.22. The outer portion

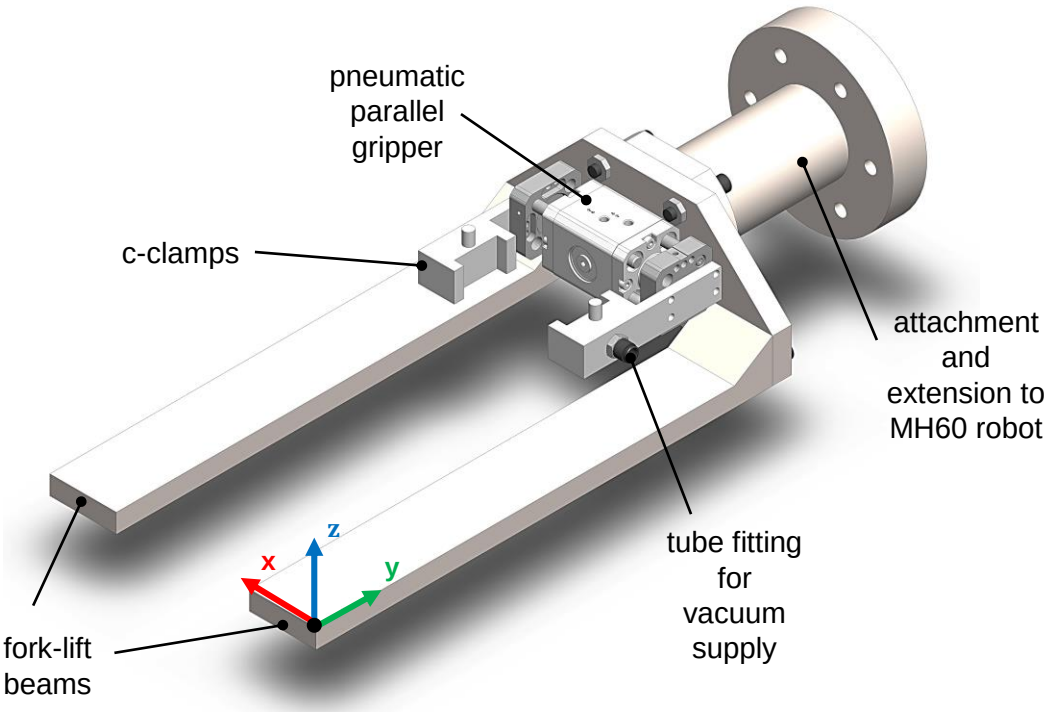

Figure 3.21. SolidWorks CAD model of end-effector design

of the hole was tapped with 1/8 NPSC pipe threads for a 1/4" tube fitting. The inner portion of the hole has a larger concentric circular groove around it that was used for attachment of a high temperature Kalrez 4079 O-ring. This O-ring was used to seal the mating of the vacuum between the left clamp and gripping block. The clamps have vertical cylindrical pins which mate on the gripping block and were used to restrict movement in the positive and negative y direction. The pins were used to improve accuracy during transport and part locating.

The end-effector's structure was designed around the Yaskawa MH50's upper arm or T-axis. The upper arm contains 6 threaded holes for end-effector attachment. The attachment piece, as seen in Figure 3.23, fitted concentrically on the end where the attachment holes were located. A cylindrical extension piece was located between the attachment and main fork lift structure of the end effector. The cylinder was hollow in order to reduce the weight of the end-effector overall. This section extends the reach of the end-effector's forks, which was necessary because of the size of the MH-50's upper arm. The large size of the upper arm could limit the robot's ability to interact with the PBP and HTE when they are being deposited inside or removed from the inside of the FDM systems. The end-effector was slender in its height (z-axis) and width (x-axis) which allows it to maneuver inside the FDM systems easily with the added extension. A middle third piece was

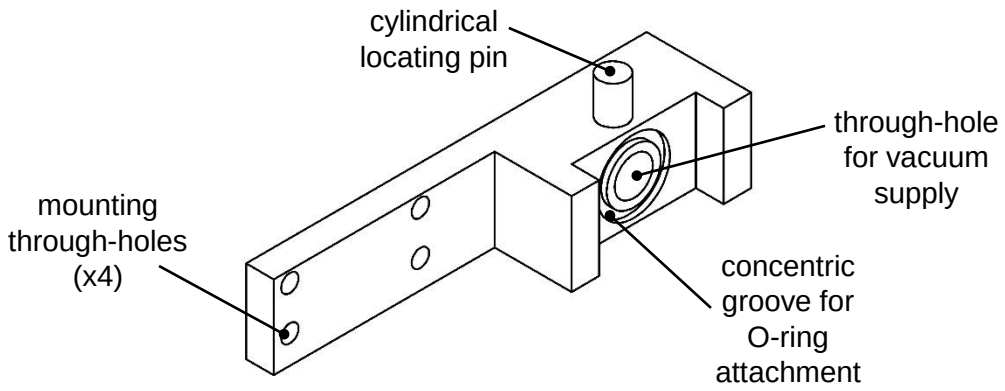

Figure 3.22. Design features of c-clamps of end-effector (left clamp with vacuum port)

used to connect the extension cylinder to the fork structure. The fourth piece contains mounting through-holes for the parallel pneumatic actuator and the two forklift beams.

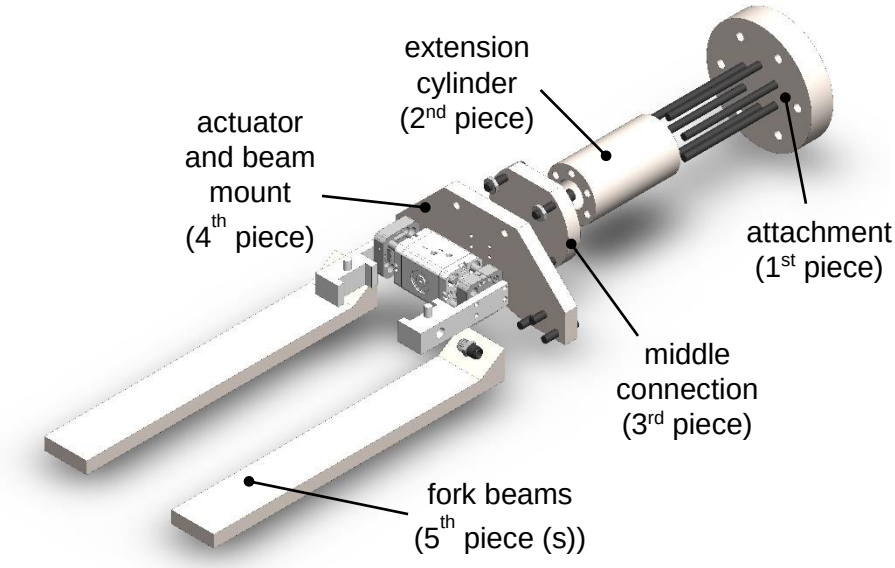

Figure 3.23. Exploded view of end-effector

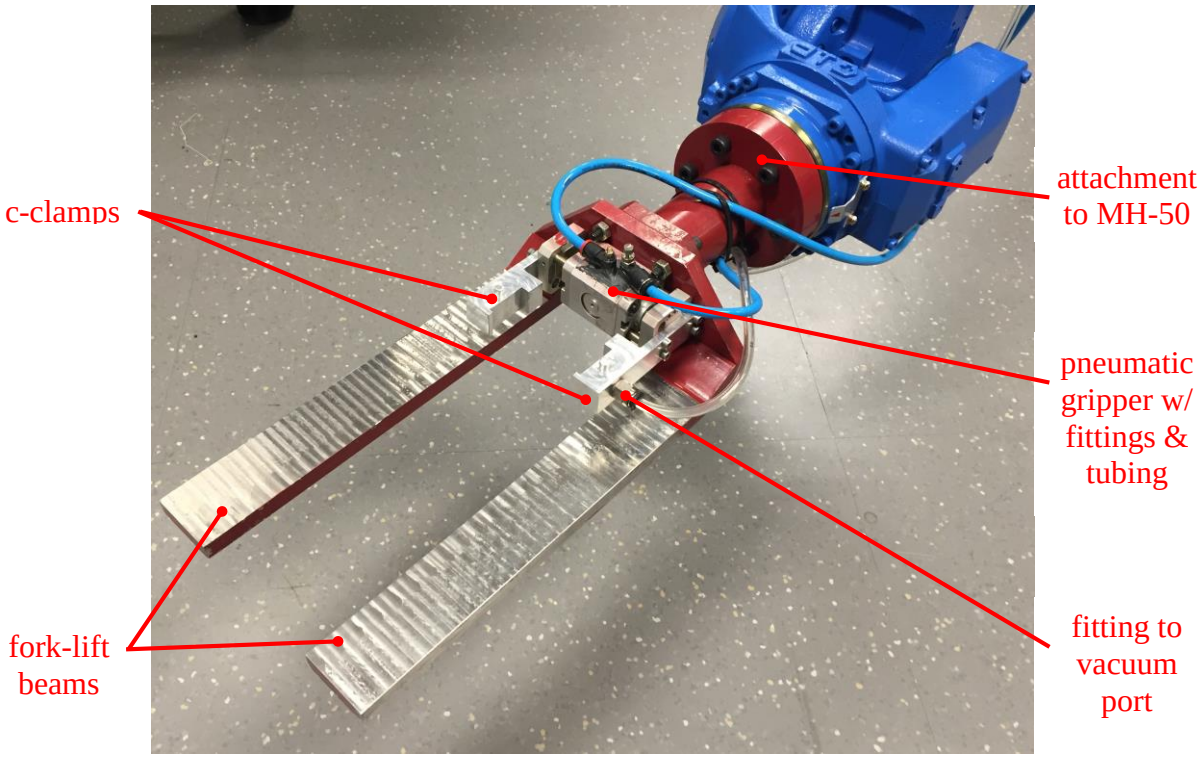

Figure 3.24. Photograph of end-effector

3.4 Material and Component Selection

The material for the structures of PBP, HTE, and end-effector were primarily chosen based on weight constraints. The end-effector's material was chosen initially to be 304 stainless steel because of its capability of bearing the loads of the PBP/HTE assembly. The weight of the end-effector was approximated to 8.16 kg according to a CAD evaluation. Considering this and the given payload of the MH50 robot to be 50.0 kg, the remaining capable payload is 41.8 kg. This weight would be the maximum load the end-effector would be required to sustain.

A loading simulation, finite element analysis (FEA), was conducted in SolidWorks 2014 on the end-effector with a load of 410 N (41.8 kg) placed on the forks' top surfaces (Figure 3.25). The fork beams and actuator/beam mount piece of the end-effector were considered as one body for the analysis. A boundary condition was added to fix the back end of the body. The analysis revealed a maximum resultant deflection of 0.48 mm (0.018") at the front edge of the forks and a maximum Von Mises stress of 30 MPa at the cornered edge where the beams begin. Comparing this stress to the yield stress of 304 SS, 207 MPa, gave a safety factor (design factor) of about 6.9 which was ideal (Budynas and Nisbett 2011). This value indicated that the forks are capable of bearing the load without failure. The deflection experienced was small but cannot be overlooked. The deflection was capable of causing the PBP and HTE to be un-level or misaligned vertically (x-y plane) when being transported by the end-effector. Although this was true, the positioning repeatability of the robot (±76 μm or 0.003") could be utilized to level the components during transportation to compensate of the offset created by the deflection.

With the maximum load verified through FEA, the materials for the structures of the PBP and HTE were chosen. In order to minimize the weight of these components, aluminum was determined as the base material to be used for their structures. The use of a steel as the base material

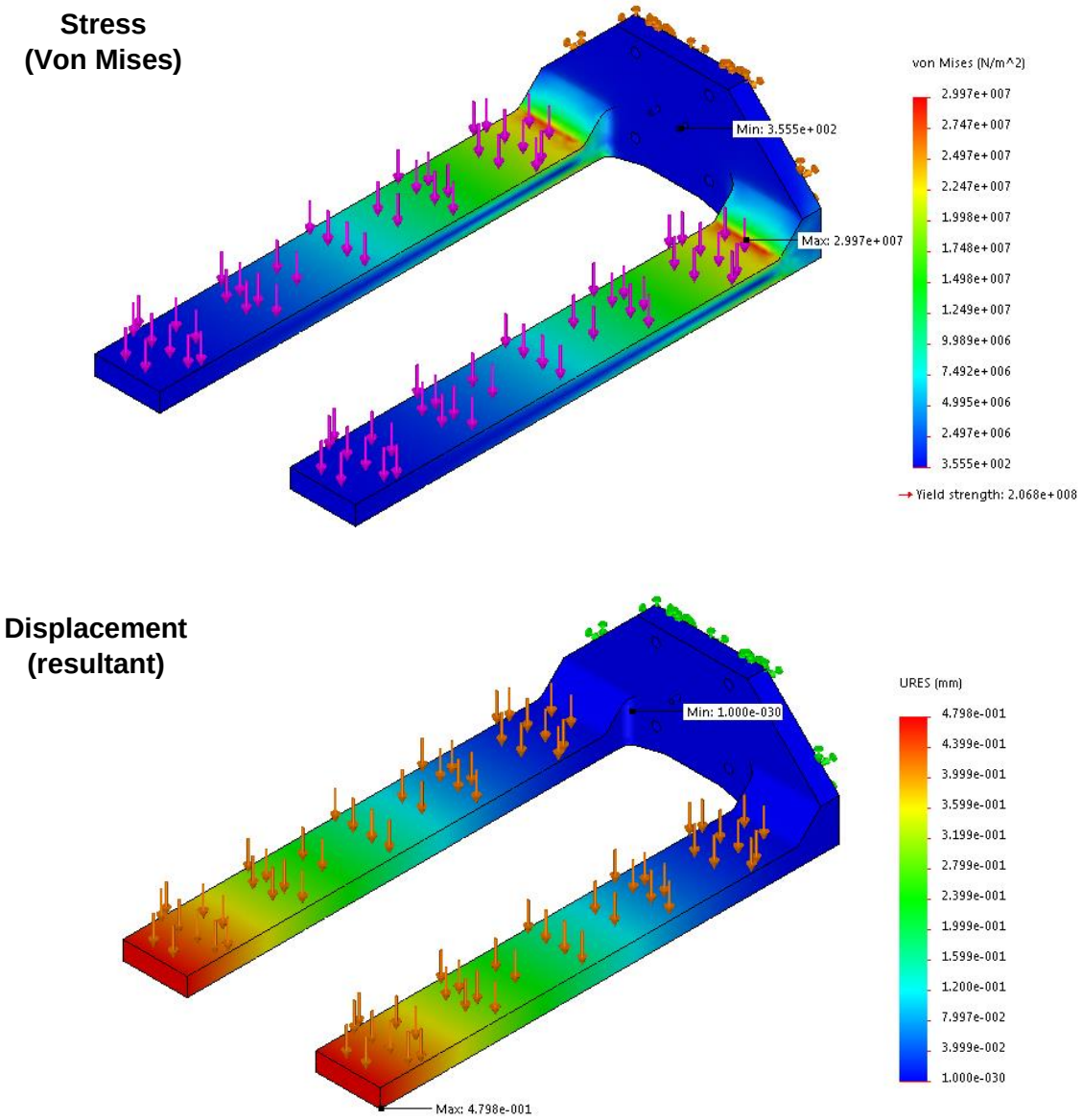

Figure 3.25. Loading simulation results from SolidWorks for Von Mises stress and resultant displacement

could cause them to exceed the payload of the material handling robot and induce positional inaccuracies, even if the end-effector was capable of the bearing their loads. The final overall weight of the HTE and PBP together was measured to be about 25.5 kg, which is about 61% of the maximum allowable payload. The remainder of the payload could be utilized for the addition

of the other components such as cameras for computer vision or pyrometers for additional temperature monitoring.

Several of the components used in the designs of the PBP, HTE, and end-effector were constrained by temperature requirements. These particular components needed to be capable of operating in temperatures close to or more than 150 °C since the envelope temperature is 145 °C when processing PC with FDM. The selected components, their base and insulting material(s) of composition, and their operating temperatures are all listed in Table 3.3.

Table 3.3. Maximum operating temperatures of components in PBP and HTE design

Component	Material(s)	Max. operating temperature (°C)
tubing and fittings (PBP)	316 SS	537
lift check valves (PBP)	316 SS	482
O-rings (PBP)	Kalrez 4079	315
curtain/bellow (HTE)	fiberglass, Teflon	260
sleeve bearings (HTE)	Rulon J	288
hot air blower, bearings (HTE)		120
insulation (HTE)	mineral wool	650
insulated wire (HTE)	PTFE, fiberglass	250
foil tape (HTE)	AL foil, fiberglass, silicon	315

The PBP was a major component of the system and was utilized in the envelope temperatures at all times. The PBP's aluminum structure has no issues operating in the high temperatures. Although, there are specific portions of the vacuum system in the PBP design that were specifically selected to endure the envelope temperatures. The tubing and fittings used to channel the vacuum air were selected to be stainless steel which allow them to operate sufficiently in the heated environments. The valves used to restrict the direction of air flow in portions of the vacuum system were chosen to endure the high temperatures as well. Lift check valves capable of the temperatures, made from 316 SS were selected. The O-rings used with the gripping block,

vacuum port, and end-effector clamp all needed to be specifically chosen as well. The O-rings are made of Kalrez 4079 material which has a maximum operating temperature of 315 °C, as seen in Table 3.3.

The design of the HTE required several high temperature capable components that could operate in its interior temperature environments. The hot air blower (AC motor) was selected first since it was one of the major components of the HTE design. Although the motor was not required to be fully encompassed in the heated environment inside the HTE, its motor shaft is exposed to the heated environment. The shaft is capable of conducting part of the heat to its bearings, which should be capable of handling the increase in temperature. The hookup wire used to apply power to the heaters inside the HTE was important to insulate to ensure its ability to provide the necessary amount of current. The curtain or bellow used was selected that was specific for oven applications and is even used in the envelope of the Fortus 400mc, as discussed in Chapter 2. The sleeve bearings used to guide the base of the curtain door were also selected for the temperature environment.

Overall, the materials and components were selected, as previously stated, based on the 145°C envelope temperature for printing with polycarbonate. Although, the maximum build envelope temperature of 225°C with PPSF was also considered as a secondary goal in the selection process. Based on the selected materials and temperatures seen in Table 3.3, this secondary goal was achieved in the majority of the components, excluding the bearings of the hot air blower. As previously discussed, the bearings will not be fully exposed to the high temperatures, which is confirmed in HTE temperature testing results shown in section 4.4 of the next chapter As a result, the 225°C temperature goal was also met, allowing for the possibility to print parts made from PPSF.

3.5 Material Handling Process

The process in which the PBP and HTE were used in handling the products of the Multi^{3D} system was significant and key to the multi-functionality of the system. When parts are transported, the PBP/HTE assembly operates so that only a small drop in part temperature occurs and vacuum is maintained to the build sheet. Figure 3.26 shows the basic process involved in depositing the PBP/HTE assembly on to the leveling plate in a FDM system. The process in Figure 3.26 could be further detailed to better understand the situation overall.

In step 1, after the door of the FDM has been actuated open, the PBP/HTE assembly is deposited into the FDM system. The vacuum fitting of the PBP mates with the vacuum port on the leveling plate to supply vacuum to the build sheet. The end-effector then actuates its gripper open to release the vacuum it is supplying and to release the PBP structure. The end-effector then slides out from underneath the PBP. In step 2, the end-effector moves to a higher vertical position and slides underneath the lifting structure of the HTE. Once the end-effector is positioned correctly, it actuates its grippers closed to restrain the HTE and then lifts it a set amount. The door of the HTE is then actuated and compressed to its open position in step 3. The compressed door principally removes the "4th" wall of the HTE so it does not collide with the 3D printed part during removal. Finally, in step 4 the HTE slides over the part and is removed from the FDM system. The door of the Fortus 400mc is then closed by its actuator and the door of the HTE is also closed. The robot places the HTE on a table where it continues to run and maintain its internal temperature. When removing the PBP/HTE assembly from the Fortus 400mc, the operations shown in Figure 3.26 are simply executed in reverse order. The PBP/HTE assembly will be used in a similar fashion when transporting parts to other stations (e.g., CNC router) of the Multi^{3D} system.

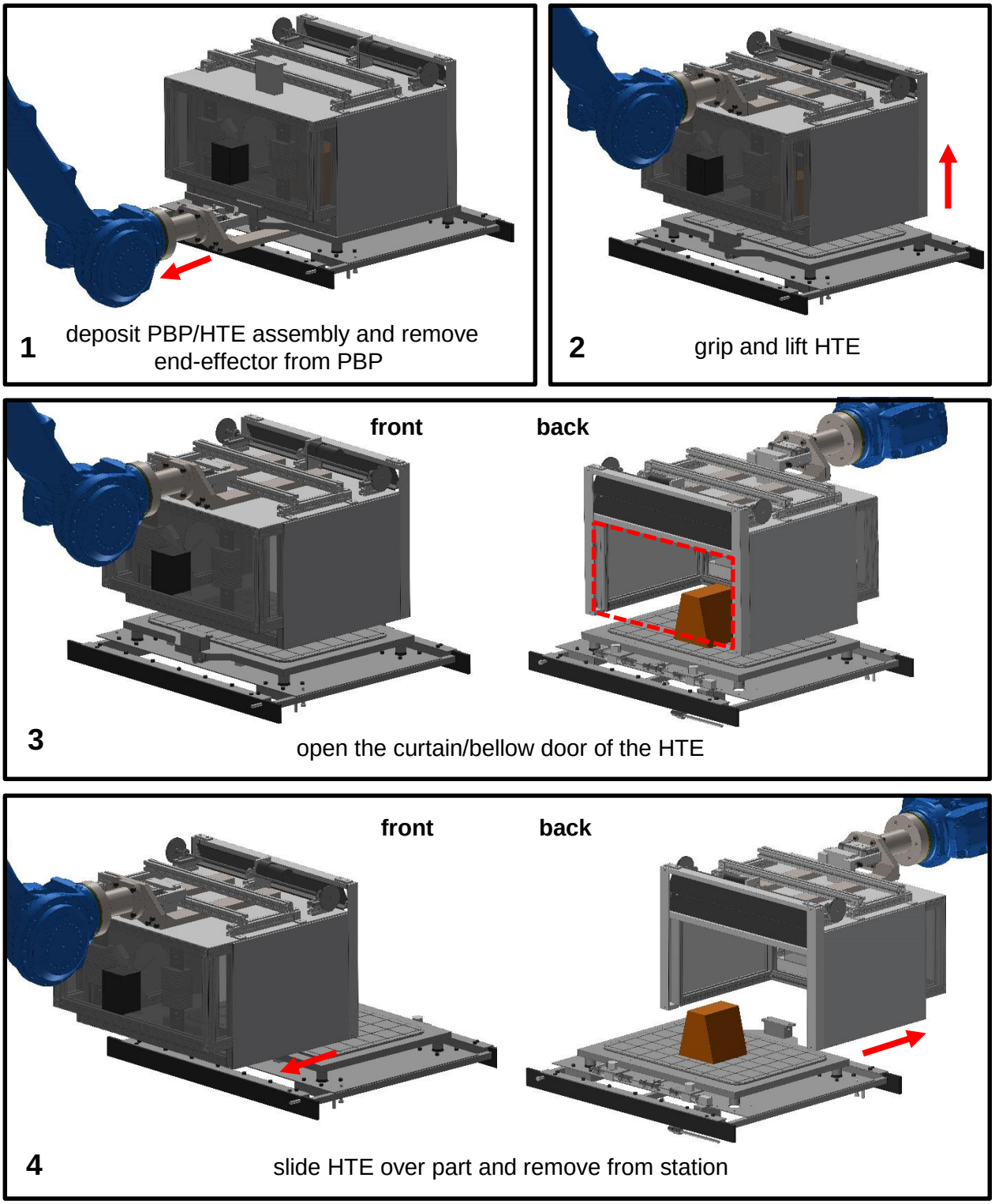

Figure 3.26. Methodology of PBP and HTE material handling process, step by step procedure for depositing PBP/HTE into the Fortus 400mc

Chapter 4

Design Evaluation/Experimentation

In order to fully evaluate the prototype designs created for the HTE, PBP, and end-effector, several experiments were conducted to evaluate these designs and their constituents. The majority of these experiments led to design changes within the prototypes. Respectively, experimentation was also conducted to demonstrate the cooperation of additive and subtractive manufacturing processes in the Multi^{3D} system. The first sections of this chapter describe the experiments conducted for design evaluation and the last section discusses a demonstration experiment.

4.1 Vacuum transition and port mating

It was important that the transition between vacuum sources on the PBP was tested to evaluate the performance of the design and its check valves. This vacuum transition testing took place early on before the leveling plate was added and modifications were made to the FDM system. As a result, the first testing was conducted outside the FDM system.

The setup of this experiment used two vacuum units, one connected to the end where the vacuum would be supplied by the manufacturing station and the other connected to the left clamp of the end-effector (Figure 4.1). The PBP was lifted and clamped by the end-effector with the clamps mated properly with the gripping block. A build sheet was cut to a custom size for the smaller build area of the PBP. The custom build sheet was then properly positioned on the PBP's surface to receive suction from the vacuum channels. The process of the experiment then began by closing the pneumatic gripper on to the gripping block and activating the vacuum unit connected to the end-effector. The build sheet was then inspected to ensure it was suctioned by the end-effector's vacuum. The second vacuum source at the back of the PBP was then activated and the suction of the build sheet was inspected once again. The grippers of the end-effector were then

actuated open to release the vacuum supply at the gripping block. The gripper was actuated several times and the suction of the build sheet was monitored. As well, the vacuum supply connected to back of the PBP was activated and deactivated several times while the end-effector gripped the PBP. No loss of vacuum was observed during the actuations of the end-effector and deactivations of the back vacuum supply. This indicated that the vacuum system, including the set of lift check valves, was working properly and transitioning well between the two separate sources.

The only issue observed during this testing was with the strength of the vacuum. The suction was not as strong as the vacuum the platen, of the Fortus 400mc, applies. The same vacuum was not experienced, approximately -33.9 KPa at least. Inspection of the tubing, fittings, and mating of gripping block and end-effector revealed no apparent leaks in the vacuum. The issue was then attributed to the temperature of the platen in comparison to the PBP during these tests. The platen is exposed to the temperatures of the FDM envelope constantly. As a result, when a build sheet is placed on the hot platen, it slight deforms and conforms to the surface of the platen. This allows the suction of the vacuum to seal better, improving the vacuum amount. Subsequently, once the PBP was working with the leveling plate inside the heated envelope of the FDM, the

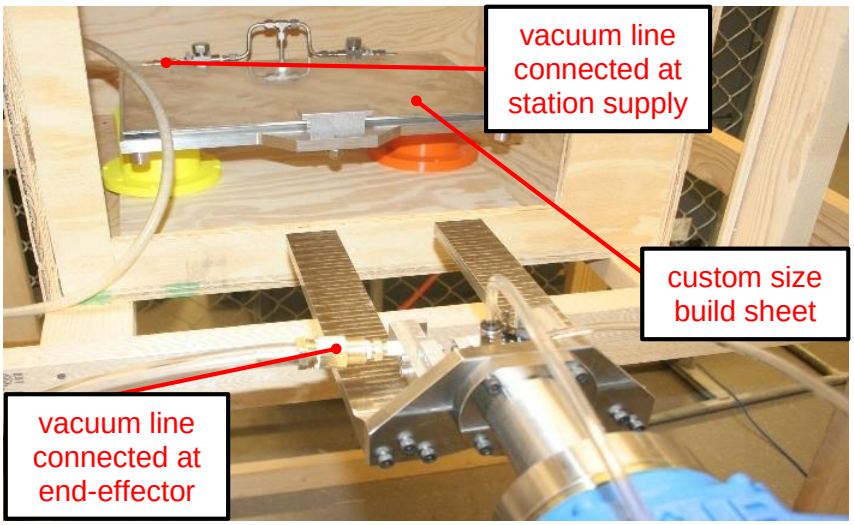

Figure 4.1. Vacuum transition testing setup

vacuum pressure was analyzed again. The pressure increase was then observed to be ideal and the same as with the platen. The vacuum gauge of the FDM showed negative pressure values between -33.9 KPa and -67.7 KPa consistently. The vacuum unit used for the end-effector indicated a necessary vacuum value of approximately -33.9 KPa or more reliably.

Prior to verifying the pressure drop of the vacuum's design, evaluation of the vacuum port on the leveling plate within the FDM took place. The design of the vacuum port was tested to ensure it mated well with the fitting of the PBP. Testing was conducted where the PBP was placed on the leveling plate manually and with the robot. The mating was monitored based on the vacuum observed on the pressure gauge of the Fortus 400mc. The mating of the PBP with the vacuum port was inconsistent. The O-ring was not fully sealing the mate with the vacuum port and air leaked at the mate. As a result, in order to combat this design issue, a spring driven design was conceived that would give the vacuum port vertical motion (refer to Chapter 3).

The new design of the vacuum port mount was manufactured and implemented but other issues surfaced with the vertical motion of the port. The SS tubing that connected the vacuum fitting to the vacuum line of the FDM was too rigid. The stiffness of the tubing restricted vertical movement of the vacuum port by causing it to bind with the walls of its housing and its guide bolts.

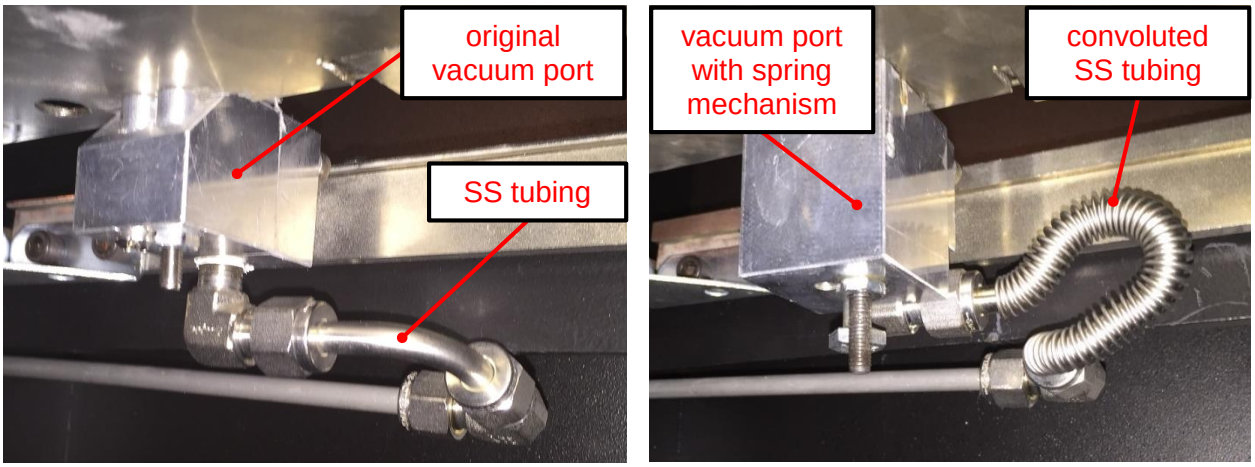

Figure 4.2. Vacuum port, original design (left) and new design (right)

As a result, the tubing between the vacuum port and FDM vacuum line was replaced with flexible convoluted SS tubing. The flexible tubing removed the binding in the motion, and mating with the vacuum port was improved with the vertical motion of the vacuum port. Figure 4.2 shows a comparison of the old vacuum port design and the new vacuum port design both mounted on leveling plate inside the FDM system.

4.2 Evaluation of PBP function with the leveling plate and FDM envelope

After the leveling plate was manufactured and mounted into the FDM system, the motion of the FDM gantry with the PBP was tested. The motion was smooth and normal similar to an unmodified FDM. The PBP was slowly raised to top of the of FDM envelope, closer to the printing head. When moved closely to the head, two particular issues were noticed in the design of the PBP. The gripping block of the PBP and back tubing structure were too tall and at risk of colliding with the top frame inside the envelope. The second observation was that the tubing and check valves positioning and mounting in the back of the PBP interfered with the range of y direction motion (front to back) of the head (Figure 4.3). Although the FDM would not ideally print in the area where the tubing and valves were located, the motion of the head when it moves to home positions

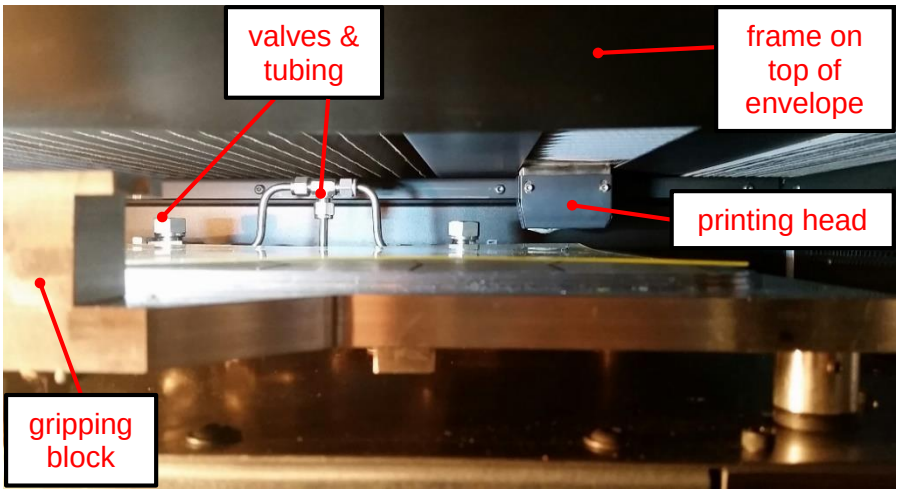

Figure 4.3. PBP deposited on leveling plate in FDM

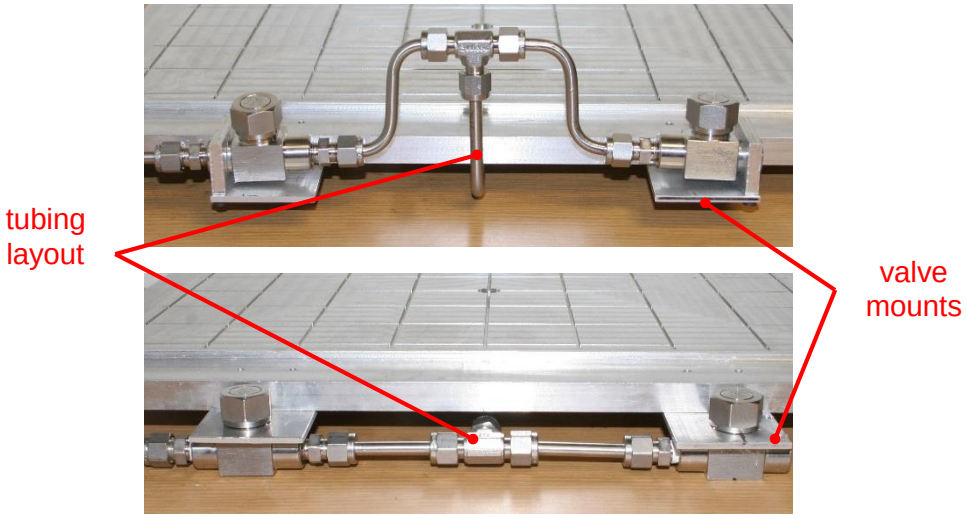

Figure 4.4. Valve mounts and back tubing, old design (top) vs. new design (bottom)

or in between building could be disrupted by placement of the tubing and valves. As a result, the design of this tubing structure was reevaluated and changed to sit lower than the build surface of the PBP. The tubing design was changed and valve mounts were modified for this design change. Figure 4.4 shows a comparison of the old design and new design.

4.3 Locating accuracy of PBP

In order to evaluate the accuracy produced by the MH50 and end-effector when transporting the PBP, tests and experiments were conducted. While initially testing the movement of the PBP with the robot, it was observed that the PBP was able to shift in the x-y plane while mated to the end-effector. The shift was observed visually and was quantified with experiments that consisted of moving the platform between a wooden mockup of a FDM system and a table with a laser displacement sensor. The PBP was completely placed and released in the mock FDM during the iterations of the experiment. The laser was positioned in two different locations on this table top: at the back and centered behind PBP (P1), and the top-left corner of the PBP (P2). Figure 4.5 shows the setup of the experiment and the two positions where the laser was placed. The two positions were used to determine the displacements experienced by the PBP in the x and y

directions. The PBP was held by the robot in the necessary position for the measurements, as seen in Figure 4.5. The PBP was moved between the mockup FDM and laser table 10 times for each position (P1 & P2) and the displacement of the platform was recorded.

The displacement data was analyzed and revealed that the standard deviation of the PBP's position was 395 µm in the y-axis and 175 µm in the x-axis. This indicates a shift in the PBP's position during transport which could cause major issues, such as collisions, when attempting to locate it within a station of the Mult^{3D} system. As a result, it was concluded that design changes were required for the end-effector clamps and gripping block. At this point in time, the circular locating pins on the clamps and notches of the gripping block were conceptualized (refer to Chapter 3). These were designed to mate during the gripping of the PBP and were used to restrict motion of the PBP during transport. As well, to further restrict motion in the x-axis, alignment bars were added to the design of the PBP which mate to the outer edges of the end-effector.

These design changes were implemented and the laser testing was repeated. The changes were validated by the comparing the data with the previous tests without the modifications. The

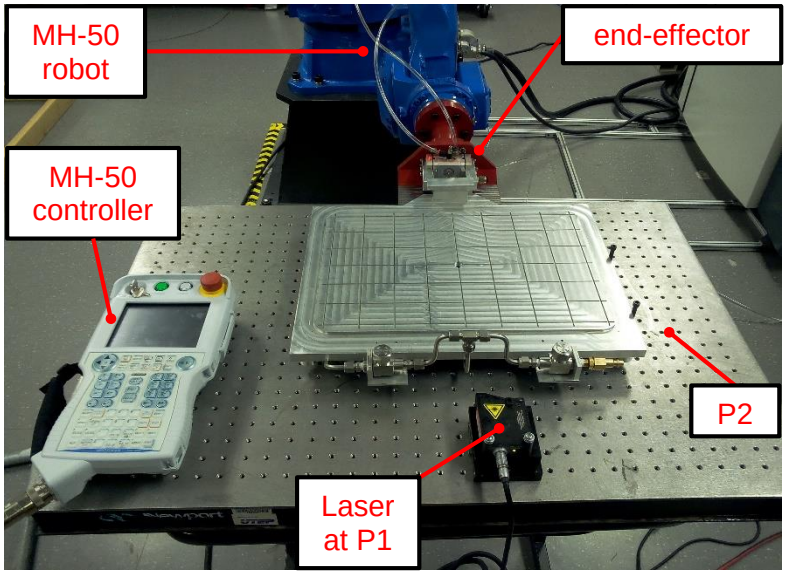

Figure 4.5. Setup for laser displacement testing

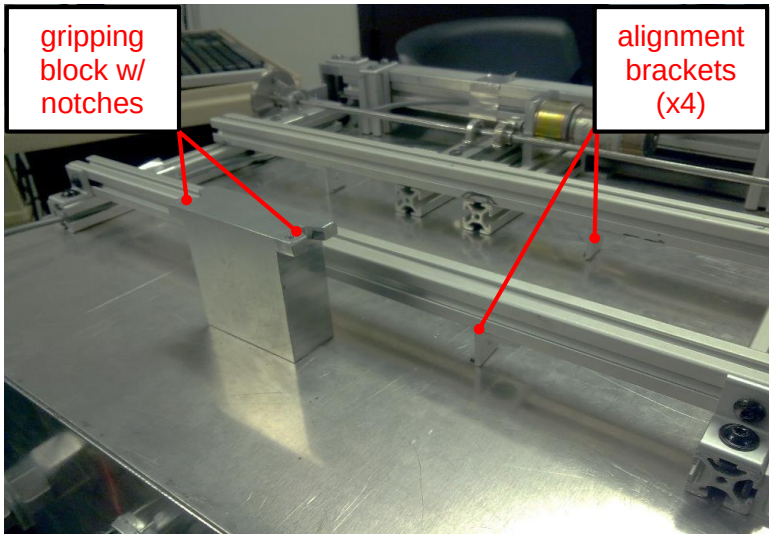

Figure 4.6. View of top of HTE, modifications made for alignment

PBP standard deviation of the PBP's positon was 15.6 µm in the y-axis and 142 µm in the x-axis, which is less than the shifts previously experienced, especially in the y-axis. This indicates that the alignment bars were effective (used compensate for x-axis shift) but not as effective as the clamp's pins (used compensate for y-axis shift). At this point, no further modifications were made to the designs. Although a larger shift was still being experienced on the x-axis, it was concluded that depositing the PBP on the leveling plate's locating pins would compensate for this shift. The locating pins would assist to finalize the alignment of the PBP when it is deposited. After this testing, the same type of setup and testing was conducted with the HTE. Similar modifications were made to the HTE which would prevent shifting. The gripping block was machined to have similar locating notches and 90 degree brackets were added to the lifting structure that would align the end-effector forks on it, similar to the alignment bars added to the PBP (Figure 4.6).

With the alignment issues resolved, experiments with printed parts to evaluate locating accuracy of the PBP on the leveling plate were conducted. The experiment consisted of printing a total of four "stair step" parts (Figure 4.7). The parts were designed to have three steps with 75 layers, 25 layers per step, and with a layer thickness of 0.254 mm (0.01"). Two of the parts were

printed without pauses, one in an unmodified Fortus 400mc and the other in the modified machine with the leveling plate. The other two were printed with pauses in between. The parts were analyzed with a Smartscope Flash 250 developed by Optical Gaging Products Inc. (Rochester, NY), a motion controlled high precision camera capable of magnifying and capturing images of the layers and measuring them. The offset of the layers was quantified by interpolating a straight line between points at the left most parts of the first layer and the last layer. This straight line was then used as a datum to measure the x-axis offset of each layer. This analysis was done with all four stair step parts.

The offset data was used to first compare "no pause" parts and draw conclusions on how well the modified FDM performed with the PBP. The data showed that the layer shifting is a range roughly of +50.8 µm and -38.1µm for both machines. Considering that the achievable accuracy of the Fortus 400mc systems is ±38 µm (±0.0015"), they were both comparable to this accuracy. As a result, the modified FDM and PBP setup does not create errors, specifically in this stair step type of geometry, greater than those of an unmodified Fortus 400mc. Now with this comparison complete, the printed parts with pauses were analyzed.

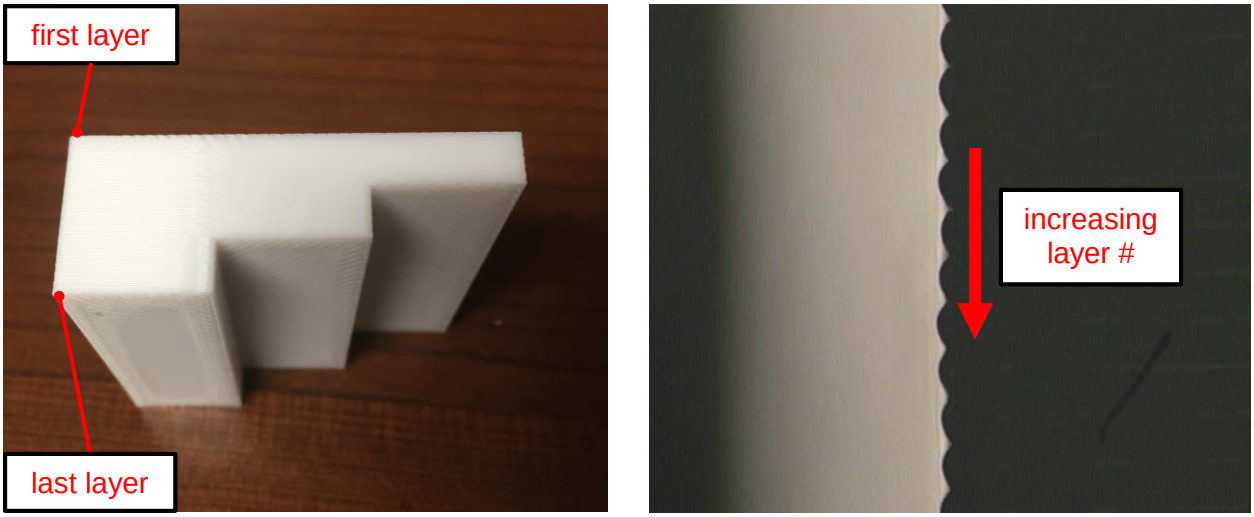

Figure 4.7. Picture of stair step part (left) and magnified Flash 250 capture of layers (right)

The pause prints were modeled to contain a total of four pauses each. The pauses were placed in particular layer positions that would allow for easier analysis. The pauses were placed at the 23rd and 48th layers (a layer before the start of next step), and 26th and 51st layers (a layer after the start of next step). During the pauses, the PBP with the HTE was removed and deposited back into the modified FDM system. For the control tests with the unmodified FDM, the builds were simple resumed after the pause without removing the building or even opening the door. From initial visual analysis of the results, there was no noticeable difference between the two. A small amount of layer shifting was visually noticeable on both parts, as seen in Figure 4.8. Offset data was then obtained from both parts and compared as well. The offset data showed that layer shifting was in the range of approximately +63.5 µm and -50.8 µm for both machines in the pause prints. Although there is a slight increase in offset when compared to the no pause parts, there is no noticeable difference between the two prints.

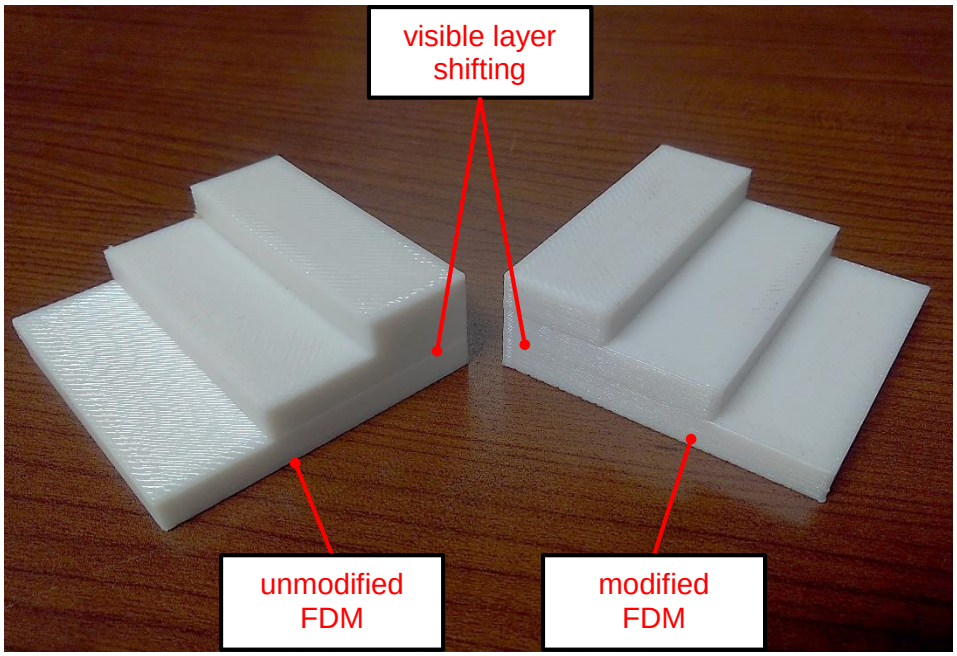

Figure 4.8. Pause stair step prints with visible layer shifting

Therefore, the data obtained indicated that the performance, accuracy wise, of the modified FDM with the leveling plate and PBP was unchanged in comparison to an original Fortus 400mc. This verifies that the locating methodology and fixture designed was capable of maintaining the necessary accuracy during deposition and removal of the PBP. Although, it was still important to note that the locating methodology was not fully repeatable and binding still occurred with the locating pins and hubs of the PBP. Future work will entail working towards improving repeatability.

4.4 HTE temperature testing, PID tuning

Experimentation was conducted to evaluate the interior temperatures of the HTE and to tune the PID controls of the temperature controller. A NI-9211 DAQ (National Instruments) temperature module was used to measure the temperatures via LabVIEW. The initial temperature testing showed that the HTE was unable to achieve the target temperature set on the controller

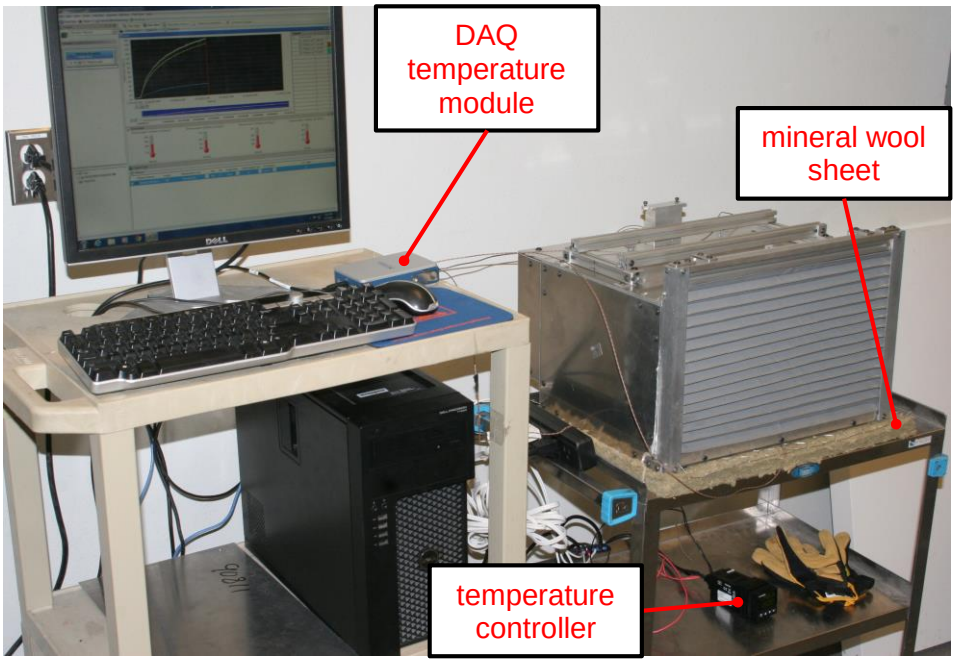

Figure 4.9. HTE temperature experimental setup

after more than an hour of running. The issue was attributed to the hookup wire used for the system. The gauge of the wire was insufficient for the required current to run the heaters at full power. As a result, the wiring was replaced with 14 AWG wire to run the heaters optimally. The setup for the experiment was also optimized so the HTE sat on top of a sheet of mineral wool insulation in order to create the most efficient interior temperatures. With the improved setup, the HTE was able to achieve the set interior temperature of 150°C within 30 min.

After the setup was improved, tuning of the PID settings commenced in order to reduce inaccuracies and fluctuations in the controllers attempt to reach target temperature. Several combinations of PID settings were experimentally tested and the most optimal setting was identified from all of the combinations. The optimal combinations being P=170, I=30, and D=3.5 which produced a fluctuation of ± 8°C (Figure 4.10). Tuning of the PID settings was not fully accurate because the constant air circulation within the envelope caused constant fluctuations in

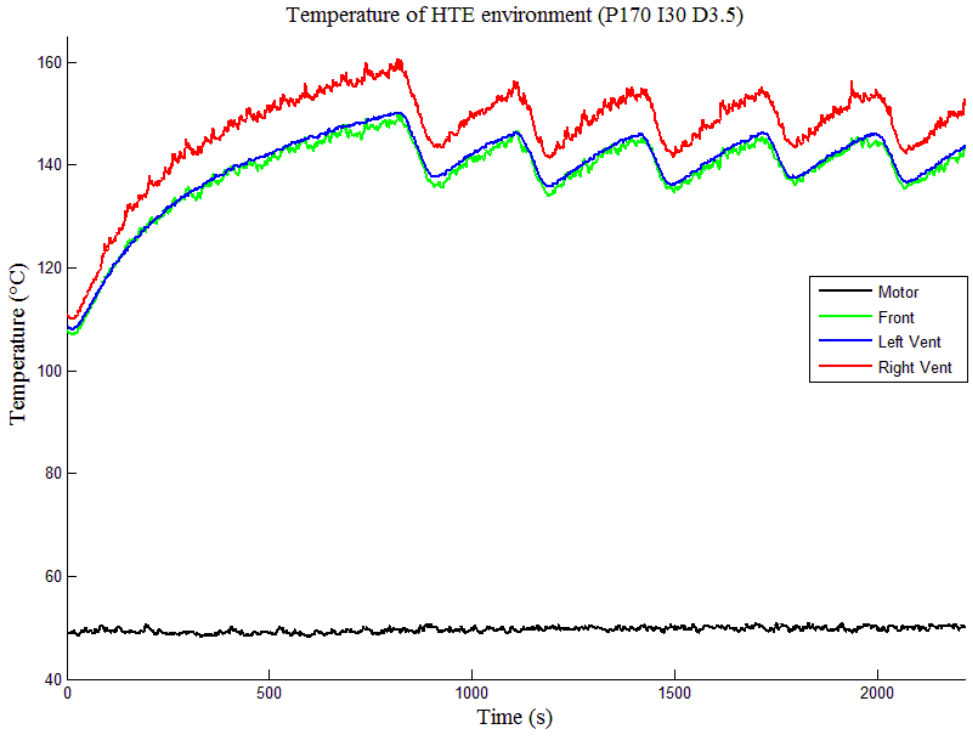

Figure 4.10. Temperature graph of HTE environment

the readings. Four temperature readings were recorded in these experiment. The temperature at the left vent, right vent, front of HTE, and hot air blower motor were recorded. The temperature varied in the interior areas of the HTE. The right vent produced the highest temperature readings. The left vent and front of the HTE showed the approximately the same temperature. Ideally, the temperature of the left vent should be equivalent to the right vent. After inspection of the setup of the experiments, the left vent thermocouple was slightly out of place most likely due to the circulating air moving it. The blower motor temperature maxed out at about 50 °C, which placed it well under its operating temperature of about 120 °C.

4.5 FDM envelope temperature drop

In order to initially evaluate the amount of temperature drop the parts could experience during their transportation through the Multi^{3D} system, a set of experiments were conducted to measure the temperature drop of the Fortus 400mc's heated envelope. The experiments were conducted by placing four thermocouples into the envelope at four points, close to the four corners of the PBP. The door of envelope was opened and exposed to ambient temperatures for one minute at a time, for three intervals. This was done to attempt to replicate the approximate amount of time the envelope would be open and exposed during a transfer process between stations of the system. Three intervals of ambient air exposure were done in order to compare and verify them with each other. The results were recorded and graphed, seen in Figure 4.11.

The results showed a maximum drop in temperature was observed at the "Right Back" position of about 12 °C. This particular piece of data was then used to compare to the temperature drop experienced in the parts during transport, discussed in the following section. As well, the data indicates varying temperature values at each of the four points inside the envelope of the FDM printer. This relationship and trends were observed to be nearly identical for all three intervals.

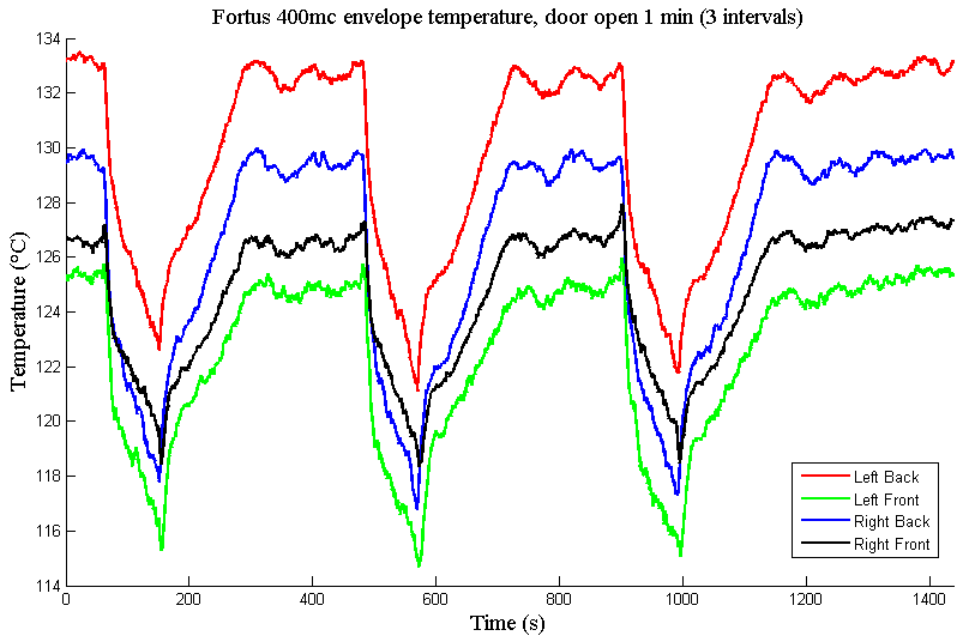

Figure 4.11. Temperature drop of Fortus 400mc envelope, three intervals

4.6 Part temperature, thermocouple embedding

Experiments were designed to test the effectiveness of the HTE in maintaining part temperature for two simple square prisms (dimensions: 50.8 mm x 50.8 mm x 5.08 mm). The experiments consisted of embedding thermocouples into two parts and recording their temperature when removing them from the FDM system after the printing process. A control test was conducted for comparison, where the parts were removed without the HTE. The experiments were organized in the following steps: 1) initialize a build, 2) pause the build half way, 3) embed thermocouples into a cavity of the build, 4) continue and complete the build, 5) start to continuously monitor temperature of part, 6) remove the PBP from FDM with heated travel envelope over the build, 7) hold the parts outside the FDM for 1 min, 8) deposit the PBP back into the FDM, and 9) monitor temperature of parts until they have reached steady state temperatures. A similar procedure was used in the control test but without involving the HTE in the process. The robot system made similar motions as to "simulate" the placement of the HTE, but the HTE was not actually used.

This was done to keep a consistent time frame, the same time of ambient exposure, between the two experiments for improved analysis.

The thermocouples were held in place at the back of the PBP and routed below it, out of the way of the end-effector. High temperature foil tape was used to hold them in place, as seen in Figure 4.12. The large length thermocouple wires were used to allow movement of the PBP during the experiments. The temperature of the parts were monitored with a similar setup as the HTE temperature experiments, with the thermocouple module. The ambient room temperature was also monitored. Two parts were used for the experiments to verify their data with one another, in case the embedding process did not work for one of them. The parts for the experiments were designed to have cavities where only the tips of the thermocouples were printed over and embedding into the substrates (Figure 4.13). In order to avoid damaging the tips of the FDM, the insulation of the thermocouples were not printed over. The fraying of the insulation could interfere with the tips and damage them during the printing process. The embedding process was successful; the thermocouples were embedded securely into all four substrate of the experiments.

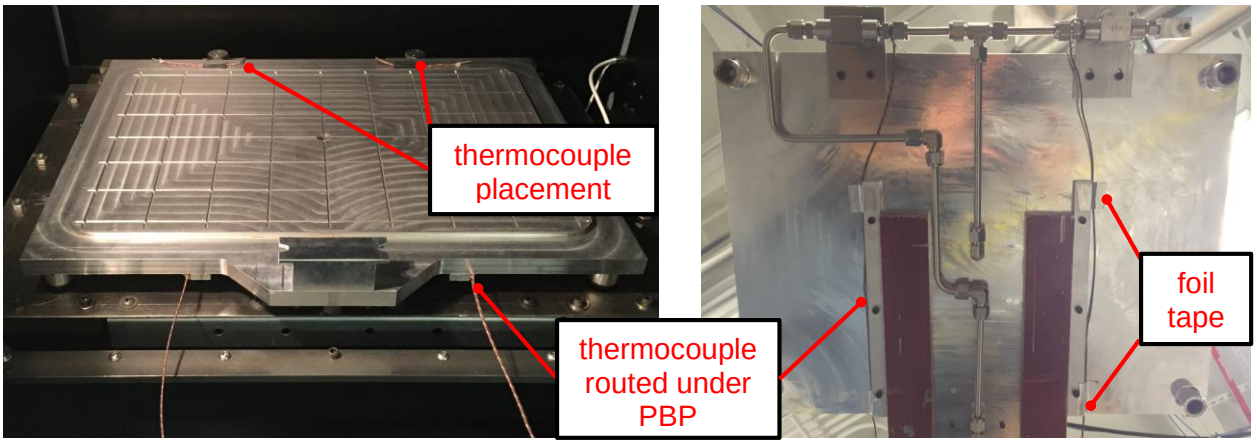

Figure 4.12. Thermocouple held to PBP prior to building

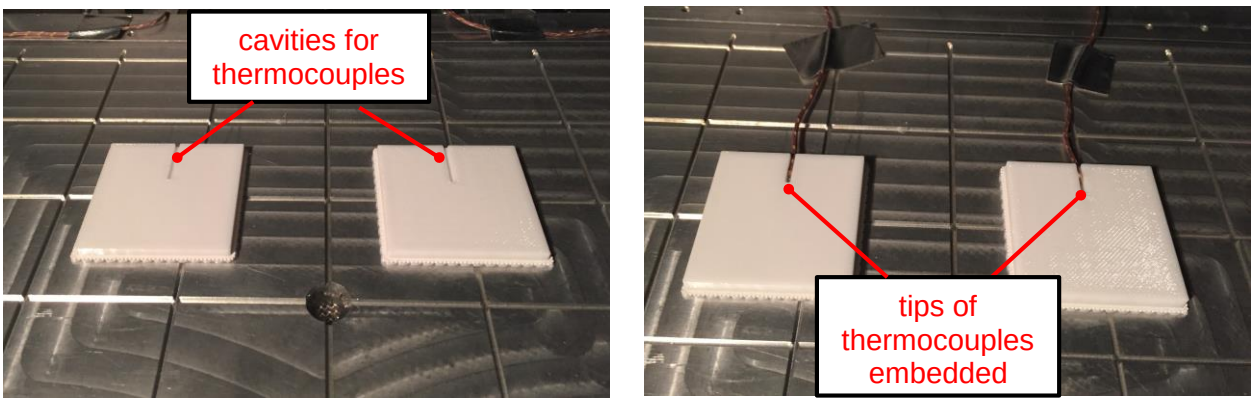

Figure 4.13. PC substrates prior to embedding (left) and after embedding (right)

The temperature data collected from the experiments were graphed and compared. Figure 4.14 shows the plotted results of the control test without the HTE. The first 120 seconds of the data represents the steady state temperature of the parts prior to removing them. The data shows a temperature drop of approximately 21°C. Figure 4.15 shows the results of the part temperature tests with the HTE used during transport. The first 240 seconds in this data represents the steady

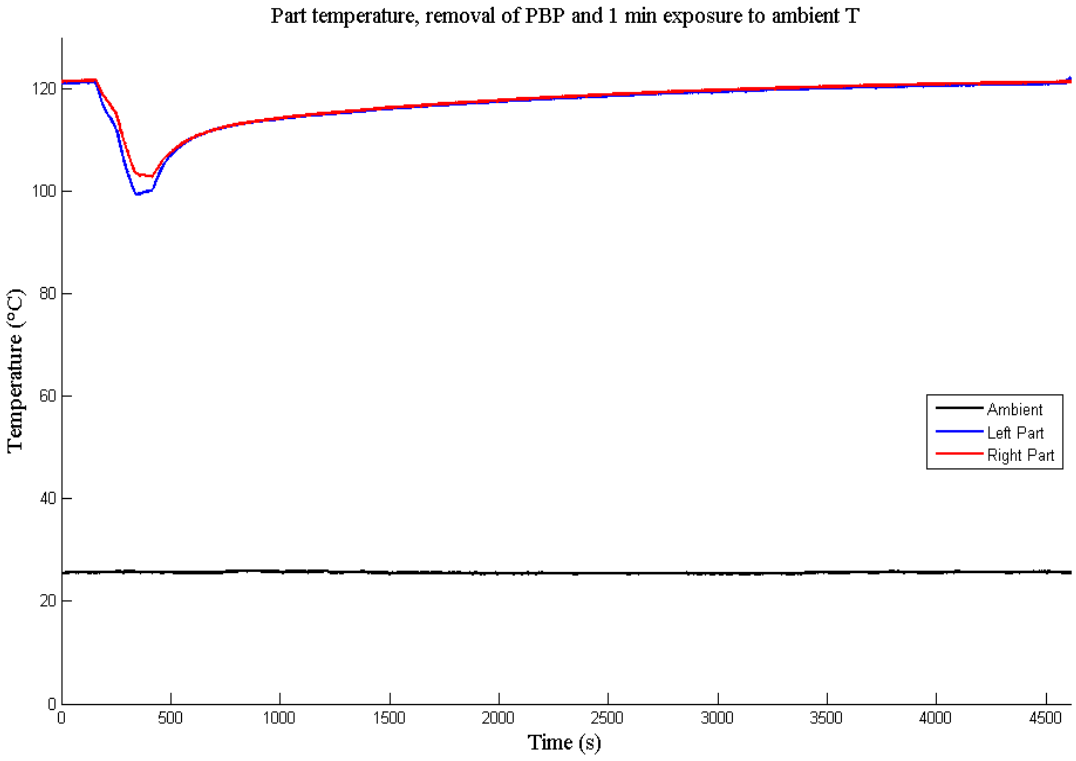

Figure 4.14. Part temperature graph of removal of part from FDM without HTE (control)

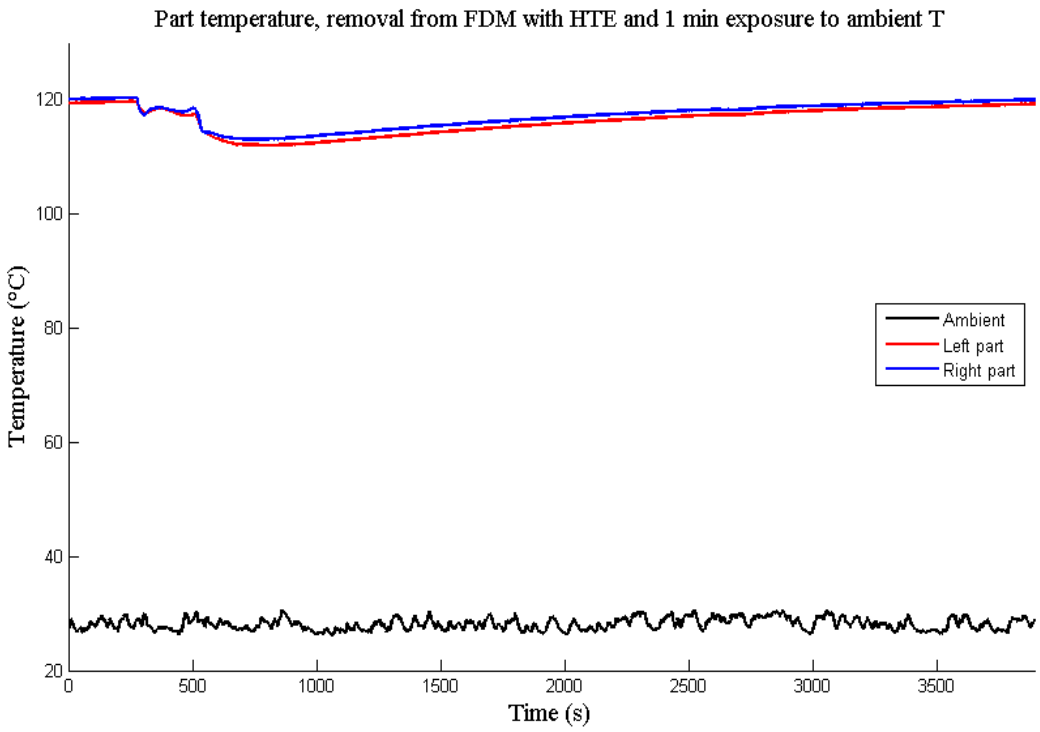

Figure 4.15. Part temperature graph of removal of part from FDM with HTE

state temperature. The part temperature drop recorded for this experiment set was approximately 6°C. These results verify the effectiveness of the envelope in reducing temperature drop of the printed parts of the system. The data from both left and right parts aligned well with one another with no major variations. The ambient temperature data fluctuated in the tests with the HTE because the thermocouple was located in an area around where the HTE sat to warm up, which increased the surrounding temperatures slightly.

In order to further analyze and characterize the results, the left part temperature data for both experiments were graphed on the same plot for further comparison. The time span was reduced to 500 s on this comparison graph to magnify the peaks and valleys for easier analysis. The peaks and valleys of the graph were characterized and compared to the positions or "events" of the experiments based on time. The temperature data was sectioned into 8 parts to identify the different events of the process (Figure 4.16.). The sections represent the following events in the

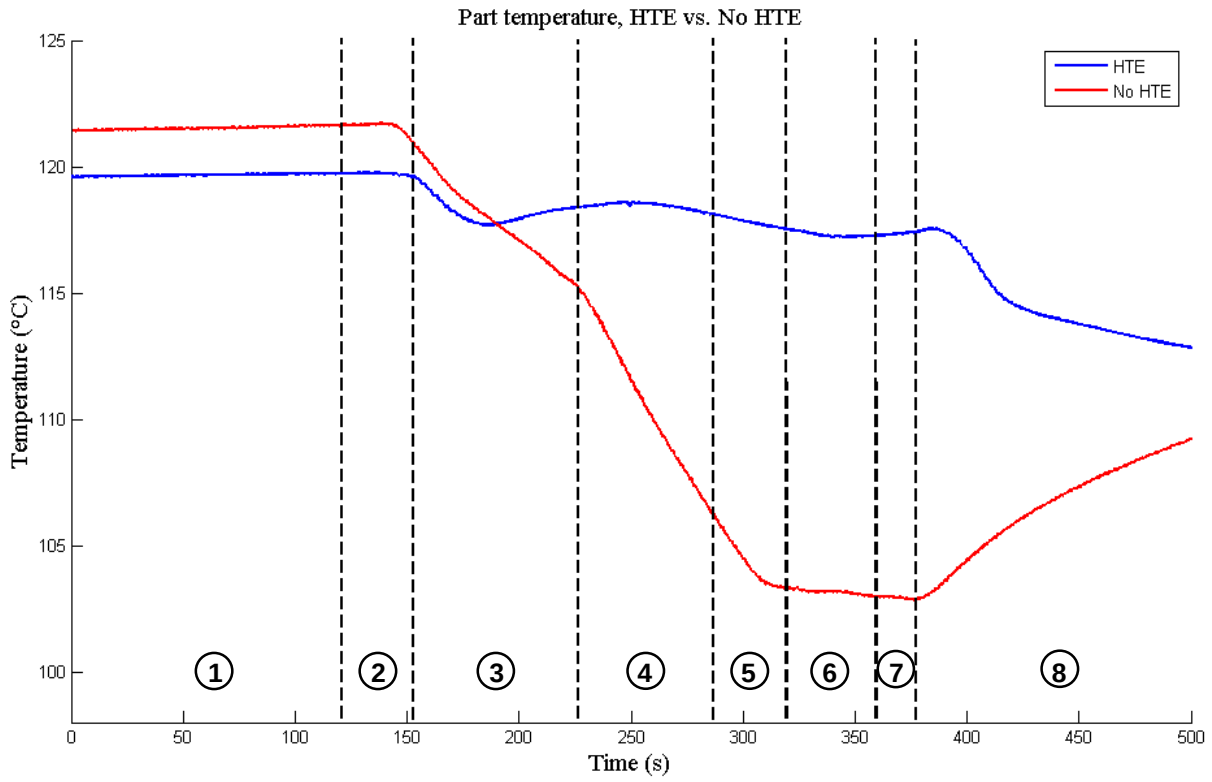

Figure 4.16. Part temperature graph of HTE vs. No HTE, with sections for timing results with the HTE: 1) two minute steady state temperature, 2) door opens and HTE is deposited, 3) PBP and HTE assembly removed from FDM, 4) 1 min period outside FDM, 5) PBP and HTE assembly deposited back into the FDM, 6) HTE removed from the part and PBP, 7) HTE outside FDM and door closes, and 8) FDM envelope heats up. The temperature results have a trend that for the most part agrees well with the event timing of the experiments. The data from the control experiment is simpler to characterize because only one major valley exists in the data that represents the time the PBP spends outside the FDM and when it begins warming up after it is deposited back. In the data with the HTE, some portions of the data were more complex to characterize.

One of the more abnormal trends seen in the data with the HTE is at events 4 and 5. The 4th event represents the minute period when the PBP and HTE assembly is left outside the envelope

and 5th is when the assembly is being deposited back. The temperature should, ideally, only be increasing or increase and then stabilize because the HTE is over the build during both sections. Instead, the data peaks and then falls towards the end of event 4 and during event 5. This drop could be attributed to the accuracy of the HTE in maintaining its interior temperature. As the results of the HTE temperature testing showed, the interior temperature of the HTE fluctuates ± 8°C from its ideal temperature. At this point in the experiment, inaccuracies in the HTE temperature may have existed or possibly in the recording process in general. When closely analyzing the data, the temperature drop is only approximately 1 °C. Another abnormal trend that occurs, is from the middle of event 6 to the beginning of 8. The temperature seems to start increasing although the HTE has been removed by this point. Once again, this could be attributed to recording inaccuracies because the increase was insignificant, about 0.3 °C.

In conclusion, the data for the two experiment sets sufficiently measured the effectiveness of the HTE during a transfer process. The data of both experiments align well with the motions and events of the process, with the exception of some abnormal but minor temperature trends. The reduction of temperature drop experienced in parts is notably reduced by 15°C overall. As well, this was compared to the temperature drop data obtained from the FDM envelope (in section 4.5), of 12 °C at most. This data value also gave indication of the amount of temperature drop the surrounding environment experiences in the process, although the envelope exposure timing from each experiment individually did not align completely, one minute compared to one minute and a half approximately. The time was not coordinated correctly because the FDM envelope temperature experiments were conducted prior to the experiments discussed in this section and a predicted transfer time was used during the data collection. As well, it was important to consider the repeatability of this experimentation and how this possibly effects the obtained data. Repetition

of this type of experiment would assist in validating the data obtained, in order to better characterize the causes of abnormalities in the data.

4.7 Demonstration: Build with machined "circuit" cavities

An experiment was designed to demonstrate an application or process that is possible with the Multi^{3D} system and its transportable material handling capabilities. The experiment demonstrated the additive and subtractive manufacturing capabilities of the system. The experiment consisted of building a part, with two pauses (3 sections) and during these pauses the part was removed and cavities were machined on its surface via the CNC router. The heated envelope, locating pin fixtures, and vacuum supply port of the CNC system were not completed at the point these experiments were conducted. As a result, the testing was designed around the inability to securely deposit the PBP within the CNC. The step by step process of the experiment was designed as follows: 1) initiate build on PBP and modified FDM system, 2) build pauses and PBP is removed from the FDM, 3) the PBP is transported via the six-axis robot and held inside the CNC and the cavities are machined, 5) the PBP deposited back into the FDM, 6) build is resumed and cavities are printed over, and 7) Steps 2 to 6 are repeated for a second pause sequence.

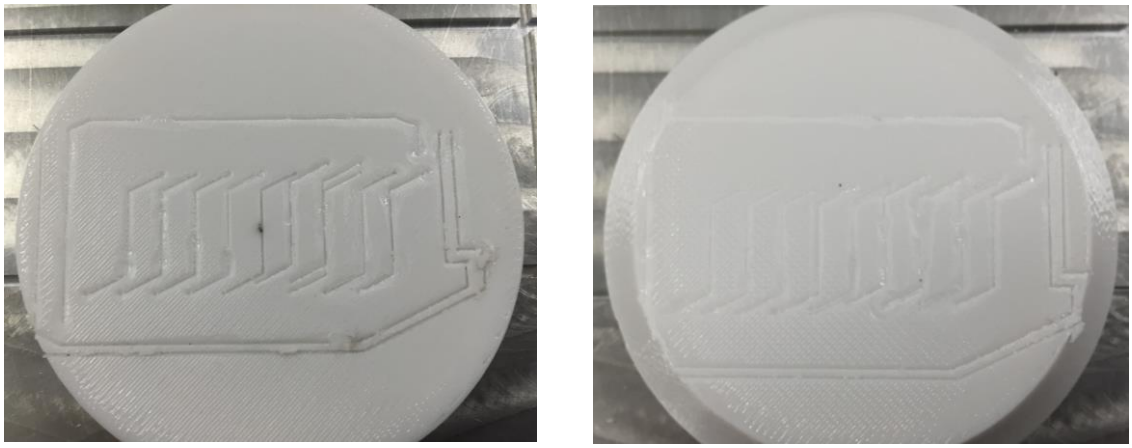

Figure 4.18. First set of cavities (left) and second set of cavities (right)

The inability to deposit the PBP inside the CNC lead to conducting the experiments by continuously holding the PBP with the end-effector while the cavity machining took place. As a result, the HTE could not be used for the process because it was not possible to remove the HTE prior to the cavity machining. The part has a short cylindrical design with its outer top rim extruded as seen in Figure 4.17. The extruded rim was incorporated into the design as a third section that could be built after the second pause which would allow the second set of cavities to be visible. The cavities were designed to resemble a circuit pattern. The cavity design was translated to G-code for the CNC router to process and a 0.02" diameter endmill was used for the machining.

Overall, the experiments were successful, but issues were encountered during the process. The cavities were machined incorrectly because of problems with the CNC router. The machining was not scaled correctly; the x-axis dimensions were observed to be double the size they were designed to be. Additionally, non-optimal feed and speeds were used during the milling process that resulting in poorly machined features. Figure 4.18 shows this stretch in the x-dimension of the cavities. Future machining processes with this CNC confirmed this speculation, eliminating the possibility of the G-code causing the error. The machined cavities were manually cleaned by

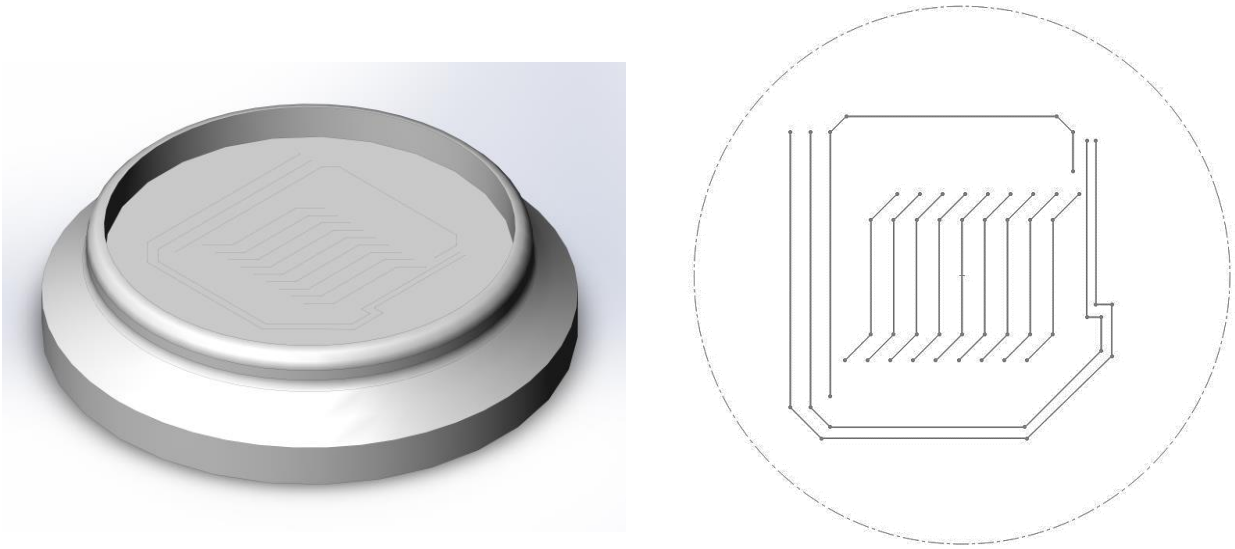

Figure 4.17. CAD model of designed part for experiment and circuit cavity design

Figure 4.19. Completed cavity part

hand with pick tools and a brush. The first set of cavities were solely cleaned in this fashion, but an attempt was made to use pressurized air to clean the second set of cavities. The pressurized air caused the build sheet to rapidly cool and as a result the build sheet lost suction to the PBP and bowed up. Thus, the build sheet was slightly shifted after the part was placed back in the FDM system, since there is no form of locating the build sheet accurately on the PBP. When the part was completed, the shift was apparent when visually examining the third section printed. As well, one layer was printed over second set of cavities unintentionally.

The cavity part was fully printed and as result could demonstrate an application of the Multi^{3D} system. The final part is seen in Figure 4.19, with one layer printed over the second set of cavities. The main observation that could be made with this experiment is that the implementation of the various design changes to the components of the material handling process allowed this demonstration to be successful.

Chapter 5

Conclusions and Future Work

5.1 Conclusions

The components for the material handling process of the Multi^{3D} manufacturing system were designed and developed. The designs of the PBP, HTE, and end-effector were conceived and manufactured. The designs were evaluated through experimentation that was created to test their functionality and determine necessary design modifications. The modifications improved the functionality of the first design iterations and a demonstration experiment was successfully conducted.

The portable build platform was successfully developed which could be removed and accurately located in a modified Fortus 400mc on its dedicated fixture, the leveling plate. The PBP included a vacuum design which allowed it to receive vacuum via two sources. One source provided by the FDM system during a printing process and another source from the end-effector which allowed it to sustain vacuum during its transfer process between machinery of the system. A port that the PBP mated with inside the FDM system to obtain vacuum was developed, tested, and modified to provide the necessary vacuum of at least -33.9 KPa to hold build sheets. The vacuum provided by end-effector was also confirmed to supply the necessary vacuum to the PBP. "Stair step" and displacement measurement experiments were used to analyze the locating accuracy of the PBP. The laser displacement studies led to certain design changes which helped restrict the motion of the PBP during movement with the robotic system. The stair step testing confirmed the accuracy of builds created with the PBP and modified FDM system to be comparable to that of the unmodified FDM system with the platen. The stair step experiments

measured layer shifting and discovered that both machines had shifting between +50.8 μm and -38.1μm without pausing the build and between +63.5 μm and -50.8 μm with pauses.

The heated travel envelope was developed capable of increasing build height (~22 cm) via its compressible door and reducing temperature drop of parts during transfer processes with the Multi^{3D} system. The HTE prototype contained a compressible bellow which actuated/ compressed via cable reeling motor system to allow it to slide over builds prior to encompassing parts within the high temperature interior. The HTE design used a temperature controller and PID controls to regulate its convective heating system to create a 150 ± 8°C environment inside its interior to replicate conditions for printing with polycarbonate. The HTE prototype design was analyzed to measure its effectiveness in reducing temperature drop in parts via experiments that involved embedding K-type thermocouples into substrates. The experiments concluded that temperature drop experienced by the substrates was reduced from 21°C to 6 °C (71% reduction) with the use of the HTE during a transfer process.

An end-effector for the Yaskawa MH-50 robotic system was also developed which permitted it to interact with the other components of the material handling process. The end-effector allowed the robot to mate with the PBP and HTE in order to transport them. The end-effector's design proved to sustain the necessary amount of weight for transporting the material handling components, 25.5 kg. The end-effector was also successful at supplying the necessary vacuum to the PBP during transfer processes, -42.3 ±8.5 KPa.

Although success was seen with the development of these material handling components, there is still room for improvement. Specifically, improvement involving the repeatability of the locating process. Otherwise, the basis of the material handling process and its components have

been developed in this work. Once the material handling process is better established, future work and experimentation with the Multi^{3D} system can take place.

5.2 Future work

Numerous accomplishments were achieved during this work and timeframe, but future work in this project in general still exists. Multi-material capabilities have not been achieved with this system at this point in time. It is inherit that the process of printing with the currently modified FDM is perfected or close to it prior to working towards multi-material parts. Material transfer processes have been successful with the current FDM machine but have not been fully repeatable. Once the repeatability of that process is improved, the second FDM technology will be rather simple to incorporate into the system using the previous modifications as reference.

Creating a more repeatable process would entail redesigning the fixture/leveling plate. The repeatability was hindered mainly by the binding of the hubs of the PBP with the locating pins. The binding would not allow the robot to remove or place the PBP repeatability. The PBP would either not deposit fully or would become stuck and difficult to remove smoothly. The source of the binding was concluded to be caused by the amount of locating pins being used in the current fixture. Future fixture designs could experiment with using less locating pins and other means of constraining the PBP, such as clamping in some form, which will reduce binding.

The efficiency of the HTE could in part be improved with some design changes. During operation, the HTE produced the required temperature environment for polycarbonate in its interior. Although, the HTE felt relatively hot to the touch on its exterior during the process. This presumably indicated that the efficiency of the HTE was not ideal, although the value was not calculated. The weight constraint was heavily considered during the design process. As a result, the decision to use 6061 aluminum in the majority of the HTE's structure was made to ensure that

it would be light weight. The use of different materials, such as steel (generally less thermo-conductive than aluminum) panels to enclose the walls, could be used to work towards improving the efficiency. The loading analysis provided in Chapter 3, section 3.4, indicates that a portion of the payload is still accessible. This allows more flexibility in material selection given the weight constraints. As well, experiments could take place with higher and lower interior temperatures. It is necessary to be able to change the HTE's interior temperature in order to allow the transport of other materials such as ABS and ULTEM 9085 for multi-material builds.

The major concentration of future work for the Multi^{3D} system in general involves the successful cooperation with its different technologies. After locating repeatability is improved with the first FDM technology, the functioning locating mechanism will be implemented into the two other machines of the system, the second FDM and the CNC router. Once this is established, the transfer process between the different machines will be coordinated. This will allow experiments to take place with multi-material parts and other processes that planned to be incorporated into the CNC router. These processes will include wire embedding and high temperature machining with the use of machine vision for registration.

References

Armillotta, Antonio. 2006. "Assessment of surface quality on textured FDM prototypes." *Rapid Prototyping Journal* 12 (1): 36.

ASTM Standard F2792 −12a. 2012. "Standard Terminology for Additive Manufacturing." *ASTM International.*

Bar-Cohen, Yoseph, ed. 2014. *High Temperature Materials and Mechanisms.* Boca Raton, Fl: CRC Press, Taylor & Francis Group.

Budynas, Richard G, and J. Keith Nisbett. 2011. *Shigley's Mechanical Engineering Design, 9th.* New York, NY: McGraw-Hill.

Campbell, Ian, David Bourell, and Ian Gibson. 2012. "Additive manufacturing: rapid prototyping comes of age." *Rapid Prototyping Journal* 18 (4): 255-258.

Cengel, Yunus A., and Afshin J. Ghajar. 2011. *Heat and Mass Transfer: Fundamentals and Applications.* New York: McGraw-Hill.

Close, Charles M, Dean K Fredrick, and Jonathan C. Newell. 2002. *Modeling and Analysis of Dynamic Systems.* New York, NY: John Wiley & Sons, Inc.

Espalin, David, Jorge A Ramirez, Francisco Medina, and Ryan Wicker. 2014. "Multi-material, multi-technology FDM: exploring build process variations." *Rapid Prototyping Journal* 20 (3): 236-244.

Guo, Nannan, and Ming C. Leu. 2013. "Additive manufacturing: technology, applications and research needs." *Frontiers of Mechanical Engineering* 8 (3): 215-243.

MatWeb, LLC. 2015. http://www.matweb.com/index.aspx.

Mellor, Stephen, Liang Hao, and David Zhang. 2014. "Additive manufacturing: A framework for implementation." *International Journal of Production Economics* 149: 194-201.

Novakova-Marcincinova, L., Novak-Marcincin, J. 2012. "Testing of Materials for Rapid Prototyping Fused Deposition Modelling Technology." *World Academy of Science, Engineering & Technology* (70): 411-414.

Rong, Yiming, and Samuel Huang. 2005. *Advanced Computer-aided Fixture Design.* Burlington, MA: Elsevier Inc.

Shulman, Holy, Drew Spradling, and Cheyne Hoag. 2012. "Introduction to Additive Manufacturing." *Ceramic Industry*, December: 15-19.

Sugavaneswaran, M, and G Arumaikkannu. 2014. "Modelling for randomly oriented multi material additive manufacturing component and its fabrication." *Material & Design* 54: 779-785.

Sun, Q., G.M. Rizvi, C.T. Bellehumeur, and P. Gu. 2008. "Effect of processing conditions on the bonding quality of FDM polymer filaments." *Rapid Prototyping Journal* 14 (2): 72-80.

Swanson, William J, Patrick W Turley, Paul J Leavitt, Peter J: LaBossiere, Joesph E. Karwoski, and Robert L Skubic. 2004. High Temperature Modeling Apparatus. United States of America Patent 6,722,872. April 20.

Tuck, C J, R J Hague, M Ruffo, M Ransley, and P Adams. 2008. "Rapid manufacturing facilitated customization." *International Journal of Computer Integrated Manufacturing* 21 (3): 245-258.

Glossary

transfer process- the process of grasping and moving the PBP, HTE, or their assembly through the ambient space within the Multi^{3D} system to allow transfer to another "station" of the system.

Appendix

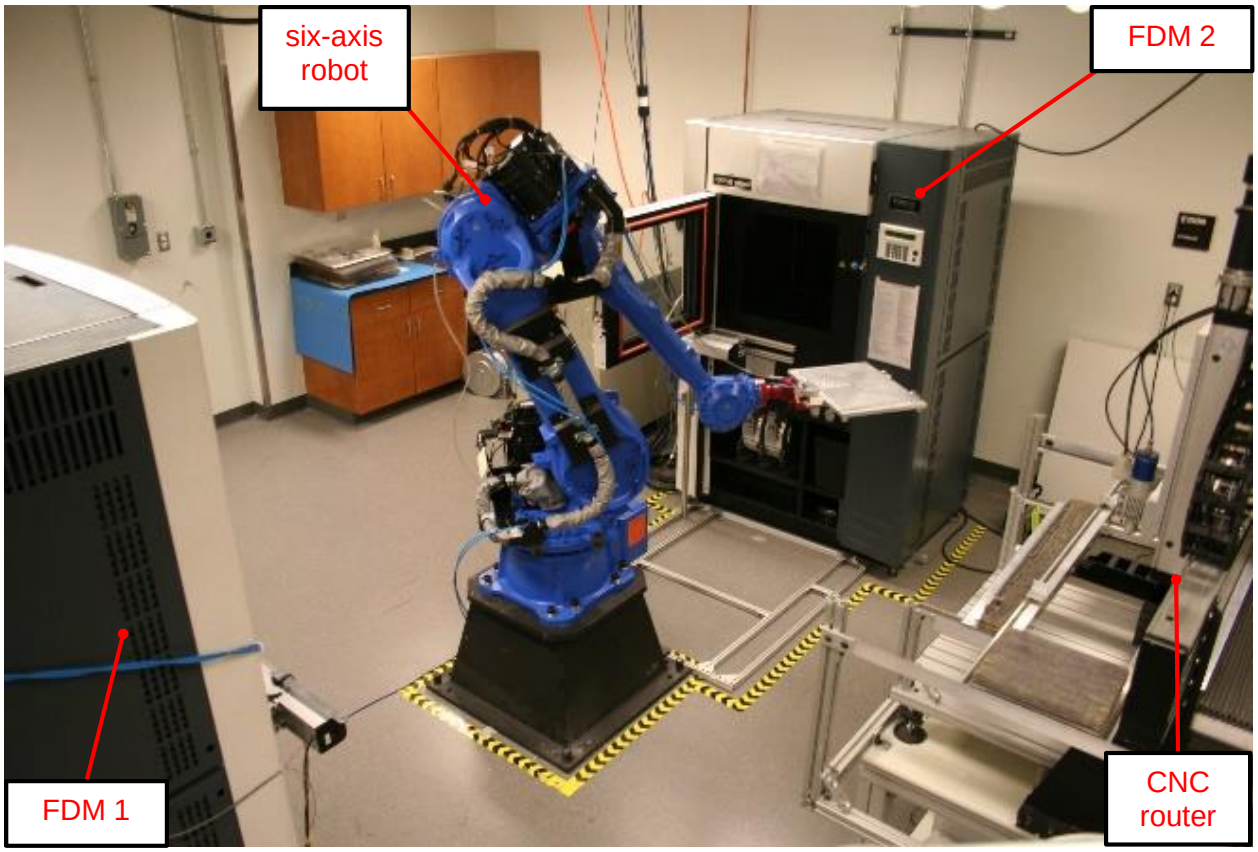

Figure A.1. Photograph of Multi^{3D} system

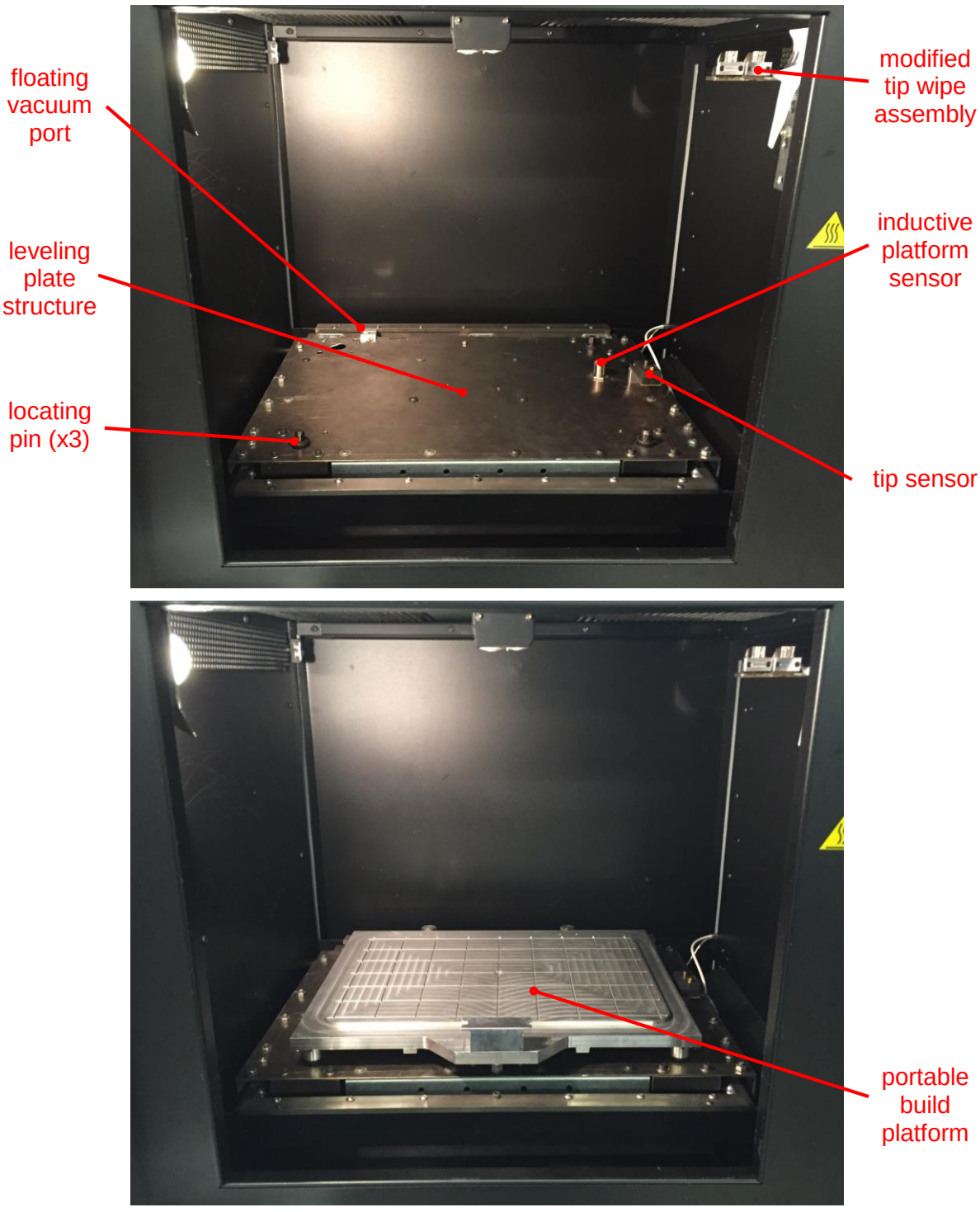

Figure A.2. Fortus 400mc envelope with modifications (top) and with the PBP mounted (bottom)

Vita

Steven D. Ambriz was born in El Paso, Texas on August 7, 1900 and is the son of Ms. Lourdes Molina and Mr. Francisco J. Ambriz. After earning a high school diploma at Canutillo High School in May of 2008, Steven began his college career at El Paso Community College. In August of 2011, he transferred his credits to the University of Texas at El Paso (UTEP). In May 2013, he obtained a Bachelor's of Science Degree in Mechanical Engineering with *manga cum laude* distinction. During his undergraduate studies, Steven was employed as an academic tutor at El Paso Community College where he tutored college students in math, science, and engineering subjects. As well, he would regularly tutor colleagues at UTEP and high school students on the weekends. As a graduate student, Steven wrote a research proposal, contributed to technical reports, and reviewed colleagues' thesis works.

Permanent address: 5877 W. Valley Cir.
El Paso, Texas, 79932

This thesis was typed by Steven D. Ambriz.